Quantum Gravity in the Lab. II. Teleportation by Size and Traversable Wormholes

Sepehr Nezami,[1,2,3] Henry W. Lin,[2,4] Adam R. Brown,[2,3,5] Hrant Gharibyan◉,[1,*] Stefan Leichenauer,[2,6] Grant Salton◉,[7,8,1,3] Leonard Susskind,[3,2,5] Brian Swingle,[9,10] and Michael Walter[11,12]

[1]*Institute for Quantum Information and Matter, Caltech, Pasadena, California 91125, USA*
[2]*Google, Mountain View, California 94043, USA*
[3]*Department of Physics, Stanford University, Stanford, California 94305, USA*
[4]*Physics Department, Princeton University, Princeton, New Jersey 08540, USA*
[5]*Blueshift, Alphabet, Mountain View, California 94043, USA*
[6]*Sandbox@Alphabet, Mountain View, California 94043, USA*
[7]*Amazon Quantum Solutions Lab, Seattle, Washington 98170, USA*
[8]*Amazon Web Services (AWS) Center for Quantum Computing, Pasadena, California 91125, USA*
[9]*Brandeis University, Waltham, Massachusetts 02453, USA*
[10]*University of Maryland, College Park, Maryland 20742, USA*
[11]*Faculty of Computer Science, Ruhr University Bochum, D-44801 Bochum, Germany*
[12]*Korteweg–de Vries Institute for Mathematics, Institute for Theoretical Physics, Institute for Logic, Language and Computation & QuSoft, University of Amsterdam, 1090 GE Amsterdam, Kingdom of the Netherlands*

In Brown *et al.* [PRX Quantum, 4, 010321 (2023)], we discuss how holographic quantum gravity may be simulated using quantum devices and we give a specific proposal—teleportation by size and the phenomenon of size winding. Here, we elaborate on what it means to do quantum gravity in the lab and how size winding connects to bulk gravitational physics and traversable wormholes. Perfect size winding is a remarkable fine-grained property of the size wave function of an operator; we show from a bulk calculation that this property must hold for quantum systems with a nearly AdS$_2$ bulk. We then examine in detail teleportation by size in three systems—the Sachdev-Ye-Kitaev model, random matrices, and spin chains—and discuss prospects for realizing these phenomena in near-term quantum devices.

I. INTRODUCTION

A. Quantum gravity in the lab

The holographic principle [1–3] is an important guidepost in our quest to understand quantum gravity. Its best-understood incarnation is the anti–de Sitter−conformal field theory (AdS-CFT) correspondence, where holography means that there is an exact equivalence or duality between two descriptions of the same system: theories of quantum gravity on the one hand and lower-dimensional theories that feature quantum mechanics but not gravity

on the other. Since some phenomena are complicated from one viewpoint but simple from the other, this provides a great opportunity for intellectual arbitrage. This opportunity has not gone unexploited, with an enormous amount of work done in the context of the AdS-CFT, for example.

In our companion paper [4], we explore a subject that we call "quantum gravity in the lab." We define this as being when the nongravitational side of the duality is physically realized as a strongly coupled quantum system in a low-energy physics laboratory; the emergent holographic gravity dual is then the "quantum gravity in the lab." In Ref. [4], we go on to explore a particular example of "quantum gravity in the lab" in the context of size winding and holographic teleportation [5,6]. The bulk of this paper is given over to a more in-depth examination of these "teleportation-by-size" examples.

We emphasize that "quantum gravity in the lab," as we define it, must involve holography. There are therefore a

number of explorations that, despite involving all three of quantum mechanics, gravity, and laboratories, nevertheless fall beyond our scope. For example, any experiment that has anything to do with the gravitational field that stops the laboratory equipment from floating off into space [7,8] is beyond our definition of "quantum gravity in the lab." While understanding quantum effects for the "naturally occurring" gravitational field is a key long-term goal, "quantum gravity in the lab" is not directly interested in any effect that involves the G that Newton discovered. In the language of AdS-CFT, the quantum hardware lives in the "boundary" and we are not interested in gravity in the boundary. We are interested in the emergent gravity in the bulk.

B. Quantum gravity in the lab and the NISQ era

The "quantum-gravity-in-the-lab" program does not need to wait for large error-corrected quantum computers. Progress can be made even in the noisy intermediate-scale quantum (NISQ) era.

For most of the long-term goals of the quantum computing community, e.g., simulating quantum chemistry, we think that the NISQ era offers the start of a road that will eventually lead to useful applications and new science. These payoffs may not be realized in the NISQ era but there are nevertheless many good reasons to start walking the relevant road. In some ways, "quantum gravity in the lab" is similar to other long-term programs that hope to eventually shed light on profound open problems in science.

However, the near-future prospects for "quantum gravity in the lab" could be better than this. In the NISQ era, it is necessary to foster the growth of quantum technologies by proposing scientific and industrial applications that require a small number of qubits and a lesser degree of fine tuning or error correction. We argue that this is also an area where the ideas of "quantum gravity in the lab" come into play, as recent developments in the theory of quantum gravity have shown that many random-looking and not fine-tuned systems possess interesting gravitational duals. Examples of such systems are the Sachdev-Ye-Kitaev (SYK) model, which has a Hamiltonian with random couplings, and some random matrix ensembles that are dual to low-dimensional gravity models. In particular, such systems are generically better understood when they have a large number of degrees of freedom, so this can make intermediate-scale experiments more interesting, as they can directly probe corrections that are otherwise hard to calculate. Moreover, the NISQ era offers at least one certainty: that we can learn a great deal about the strong coupling dynamics of various toy quantum models. The issues at play in that context, including questions of chaos and thermalization, are all closely connected to deep issues in quantum gravity.

C. Overview of results of this paper

The remainder of this paper is devoted to a detailed study of one example of "quantum gravity in the lab," building on our companion paper [4], in which we propose a new mechanism for teleporting quantum information ("teleportation by size") inspired by traversable wormholes in gravity and introduced the concept of size winding. In this paper, we present a comprehensive set of examples in which teleportation by size and size winding can be implemented and studied in detail, such as the SYK model, a random matrix model, and a chaotic spin chain. We use these examples to illustrate general features of the teleportation-by-size protocol and to give a clear illustration of the size-winding phenomenon at low temperatures.

In Sec. I E, we review the basic definitions and concepts introduced in our companion paper [4]. In particular, Fig. 4 shows the teleportation-by-size protocol. Readers familiar with the ideas from Ref. [4] should feel free to skip this section.

In Sec. II, we study in detail several example systems. In Sec. II A, we discuss teleportation by size at infinite temperature and then exhibit a weak version of the size-winding phenomenon at low temperatures that enhances the teleportation capacity. In Sec. II B, we present analytical results on state transfer in chaotic spin chains and again establish a link between size distribution and teleportation. In Sec. II C, we study Brownian evolution, where the Hamiltonian changes in time, and analytically study the growth of size operators. In Sec. II D, we present explicit results for teleportation by size and size winding in the SYK model at finite temperature. We further discuss the large-q limit of the model and the potential connection to stringy effects in the bulk.

In Sec. III, we discuss in detail the holographic interpretation of our protocol, especially in the context of the SYK model. This material is a nontrivial extension of the discussion in our companion paper [4]. We specifically revisit and clarify the role of size-momentum correspondence in the size-winding phenomena and elaborate on geometric interpretations of different teleportation regimes.

In Secs. III and II D, we observe that size winding can be used to roughly model the manifestation within the boundary system of the bulk radial direction. Indeed, we see that the winding size distribution mimics the momentum wave function of a particle falling into the wormhole; hence its phase describes the particle location in the bulk. In this picture, the coupling e^{igV} is similar to a shift of location, moving the particle from the left region to the right one (for a pictorial demonstration, see Fig. 1 and for precise arguments, see Sec. III and Refs. [6,9]).

The traversable wormhole is a geometrization of the Hayden-Preskill protocol [6], which in turn is closely related to the black-hole information paradox. Recently,
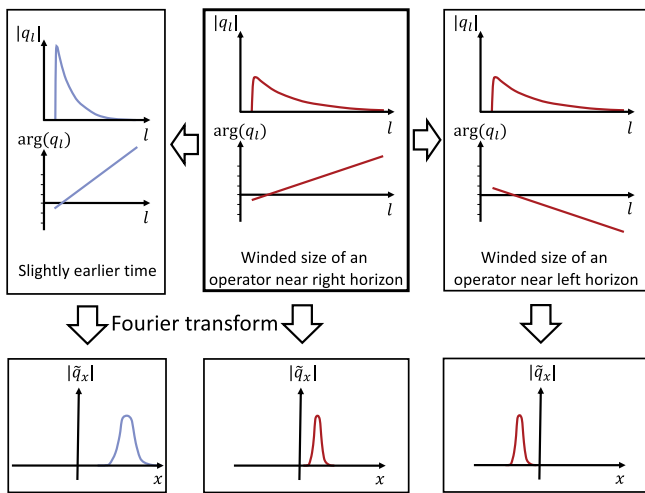
FIG. 1. The refinement of size-momentum duality to the level of wave functions. If the expansion of the time-evolved thermal Pauli (or fermion) is $\rho_\beta^{1/2} P(t) = \sum c_P P$ (or $\rho_\beta^{1/2} \psi(t) = \sum c_u \Psi_u$), then one can define the winding size distribution $q(l) = \sum_{|P|=l} c_P^2$ (or $q(l) = \sum_{|u|=l} c_u^2$), in contrast to the conventional size distribution $\sum_{|P|=l} |c_p|^2$. We argue that the q_l is the boundary analog of the bulk momentum wave function. The plot is the schematic drawing of the winding size distribution in the SYK model, near, but slightly before, the scrambling time. This is the regime where the width of the distribution is of order n. One can observe that the Fourier transform of the winding size distribution mimics the behavior of the position of the infalling particle (measured, e.g., from the black-hole horizon). Top center: the magnitude and phase of the winding size distribution. Bottom center: the Fourier transform (or bulk location) is near the origin. Top left: the magnitude and phase of the winding size distribution at a slightly earlier time. The size distribution is smaller and winds faster. Bottom left: the Fourier transform (or bulk location) is further from the origin. Top right: the size distribution after acting by e^{igV}, with the proper value of g. The distribution is now winding in the opposite direction. Bottom right: the Fourier transform shows that the particle is on the other side of the origin, a manifestation of the fact that the infalling particle has moved from one side of the horizon to the other side.

major progress has been made in resolving the information paradox (for a review, see Ref. [10]). The central ingredient in the recent progress has been an application or refinement of the quantum extremal surface (QES) formula in a regime where quantum effects are large and a bulk derivation of this formula from the replica trick. This formula delineates when information can be recovered from a black hole. Applied to our context, it gives a nontrivial bound on when the traversable wormhole protocol can succeed. We suggest a relatively simple setup where an experimental measurement of certain von Neumann (or Renyi) entropies could be used as a nontrivial experimental check of the QES formula in a regime where quantum effects are important. Our setup just involves measuring the entropy of a

subset of the degrees of freedom of a one-sided system in the thermal state. This is presumably simpler experimentally than measuring the entropy in time-dependent examples.

We conclude in Sec. IV with a discussion of possible benchmarks for building a traversable wormhole in the laboratory.

In Appendix C 4, we show that the large-q SYK model exhibits near-perfect size winding at low temperatures, where its holographic interpretation is best understood. At finite temperatures, the large-q model is still tractable and we demonstrate a rather precise match with stringy expectations. Indeed, this is to a large extent simply a translation of existing results on two-point functions for traversable wormholes [6,11] in the language of size, as we discuss in Sec. III. Although perfect size winding might be specific to systems with good holographic duals, we expect to see imperfect winding even in nongravitational systems (in Sec. II A, we show that random nonlocal Hamiltonians exhibit weak size winding, which shows that traces of geometrical wormhole physics can exist in very generic quantum systems).

D. Related work

Other studies of information transfer through traversable wormholes and related notions include Refs. [12–15]. In particular, one small-scale experiment with trapped ions has already been carried out [16] based on Refs. [17,18]. This experiment has implemented a probabilistic protocol and a deterministic Grover-like protocol [17]. In the deterministic case, the circuit in Ref. [16] can be related to our Fig. 4(a) if we specialize to infinite temperature, push the backward time evolution through the thermofield double, and replace V by a projector onto a Bell pair. Another recent experimental investigation has looked at a similar scrambling circuit but in a qutrit setting [19].

E. Review of our companion paper

In this section, we review definitions and concepts presented in Ref. [4]. Readers familiar with that work may skip this summary section.

Our starting point is the thermofield double (TFD) state on two Hilbert spaces indexed by L and R. We further assume that the Hamiltonians of L and R are the transpose of one another and that the entire LR system has a holographic gravitational dual (e.g., the Hamiltonian could be that of the SYK model). The gravitational dual of the initial TFD state is a wormhole geometry connecting L and R subsystems (see, e.g., Ref. [20]).

The presence of the wormhole in the geometry dual to the TFD does not imply that messages can be sent between the left (L) and right (R) systems. Indeed, a message sent through the wormhole from one boundary system cannot reach the other boundary and it instead meets its fate in the
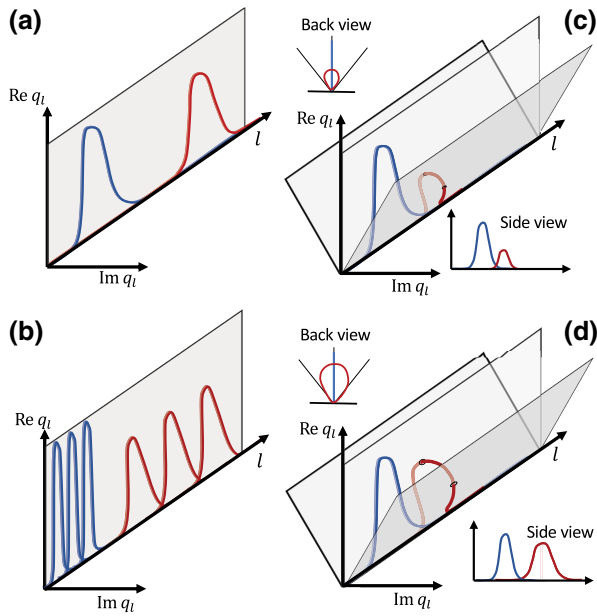
FIG. 2.   A short summary of teleportation by size, discussing different systems, different patterns of operator growth, and the consequence of each growth pattern for signal transmission. (a) Operator growth, late time, most quantum systems: teleports one qubit through state-transfer mechanism; sgn(g) independent; infinite temperature. (b) Operator growth, intermediate time: chaotic spin chains, random circuits; teleports many qubits through state-transfer mechanism; sgn(g) independent; infinite temperature. (c) Size winding (damped), low temperature: teleports through *state-transfer* mechanism; weak sgn(g) dependence; works weakly for "operator transfer." (d) Perfect size winding (not damped), low temperature: could teleport through *state-transfer* mechanism; strong sgn(g) dependence but limited fidelity; works perfectly for "operator transfer" slightly before scrambling time; strong signature of a *geometrical wormhole*. Blue, initial operator-size distribution; red, operator-size distribution of the time-evolved operator.

singularity. In that sense, the wormhole is *not* traversable and it cannot be used to transmit signals between the boundaries.

By simultaneously acting on the two boundaries by a finely tuned interaction at $t = 0$, Gao *et al.* [5] have shown that one can render the wormhole traversable. The effect of acting with the carefully chosen bipartite coupling proposed in Ref. [5] is that a negative-energy shock wave is created in the bulk, which is able to pull a signal out of the wormhole, thereby delivering it to the other boundary (for an illustration, see Fig. 3). Thus, the *LR* coupling modifies the geometry of the wormhole in such a way that a signal falling freely from one boundary can escape the singularity and reach the other boundary.

In the above story, an exotic two-sided coupling produces a negative-energy shock wave, which renders the *LR* wormhole traversable, thereby allowing a message to be transmitted from one side to the other. This explanation

of the signal transmission is given from a purely bulk gravitational perspective and it does not make clear the way in which information can be transmitted between the *L* and *R* Hilbert spaces in the dual quantum picture. In Ref. [4], and further expanded in this paper, we explain this communication phenomenon from the quantum mechanical boundary perspective. As discussed in Ref. [4], the traversable wormhole communication protocol described above can be given a boundary interpretation, illustrated as a quantum circuit and shown in Fig. 4. Moreover, the process of sending and receiving signals corresponds to a form of state transfer or quantum teleportation on the boundary [4].

We argue that the information transmission through the boundary circuit (Fig. 4) can be understood with a proper analysis of the size distribution and spreading of the operators involved. Hence, we coin the term *teleportation by size* to describe the different ways in which the wormhole circuit can be used to transmit signals.

As previously observed, there are *two* mechanisms of transmission with the wormhole circuit:

(1) *Late-time high-temperature teleportation.* This mode of transmission is—to a large extent— unexpected from the gravitational point of view and it does not immediately correspond to a signal traversing a semiclassical wormhole. It can be used to teleport a qubit at high temperatures when the system is described by (potentially nonholographic) chaotic Hamiltonians. We study this model in Ref. [4] and provide fidelity bounds for the corresponding teleportation protocol. Here, we show how it can be used to teleport many qubits in spin chains, Brownian circuits, and Hamiltonians with independent identically distributed random matrix elements.

(2) *Low-temperature through-the-wormhole transmission.* This mode corresponds to the transmission of signals through a semiclassical wormhole. On the boundary, the transmission can be understood using the size distribution of thermal operators. More precisely, we argue that the size distribution of the operators should *wind* in the complex plane, i.e., obtain a phase that is linear in the size. This phenomenon—which we call *size winding*— is at the heart of signal transmission through the wormholes. The role of the *LR* coupling is to undo the complex winding of the size of the operator and instead wind the size distribution in the opposite direction. In effect, this reversal of the winding direction corresponds to mapping the operator inserted in one boundary to the other boundary (for more details, see Fig. 5 and Ref. [4]). We explicitly show *size winding* of thermal operators near the scrambling time for the SYK model and we conjecture that the
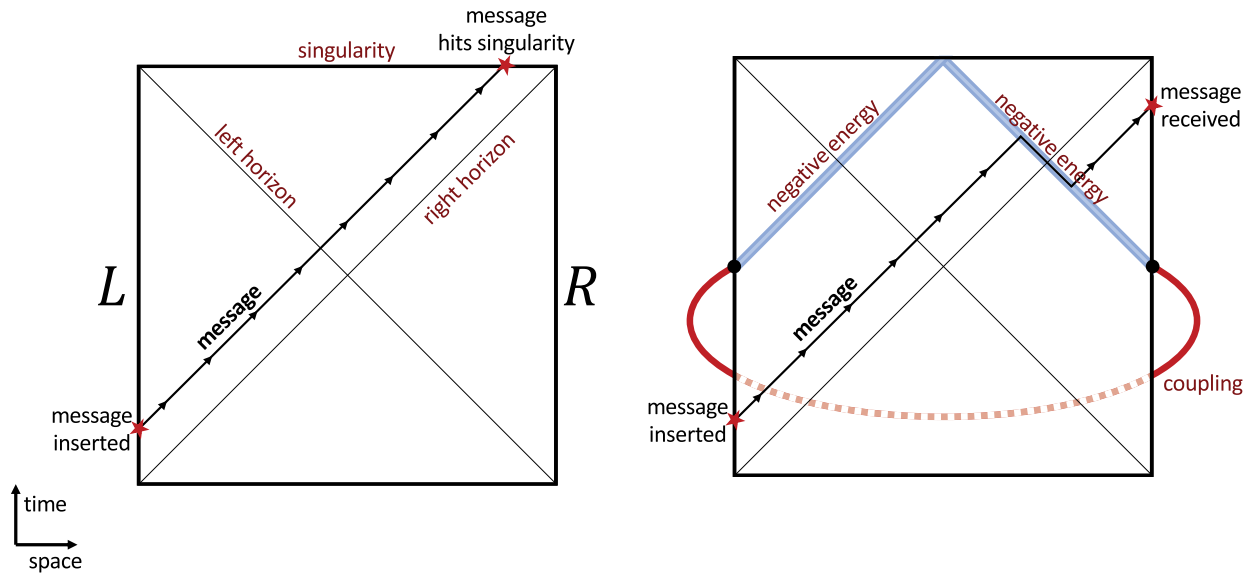
FIG. 3.   The Penrose diagram of wormholes. Left: without the coupling, a message or particle inserted at early times on the left passes through the left horizon and hits the singularity (the top line of the diagram). Right: in the presence of the left-right coupling, the message hits the negative-energy shock wave (the thick blue line) created by the coupling. The effect of the collision is to rescue the message from behind the right horizon.

phenomenon can also be found in other holographic systems. Specifically, the size distribution behaves similarly to the (null) momentum wave function in the bulk and its winding rate is dual to the "location" of the infalling operator in the bulk. In Sec. III, we expand the arguments of Ref. [4] and further elucidate the gravitational picture as well as connections to the recent developments on "gravitational islands" [21].

In this paper and Ref. [4], we assume that the total number of qubits (or fermions) on each side is n and the number of *message* qubits (or fermions) that are transmitted by the state-transfer or operator-transfer protocols is m. Furthermore, the coupling is assumed to act on k *carrier* qubits (or fermions). Unless otherwise stated, we assume that $k = n - m$, i.e., the coupling acts on all qubits except the message qubits. One can also consider $k = m$; the difference between the performance of these cases will be insignificant in the regime of interest, $m \ll n$.

1. Size winding

Before proceeding, let us review the definition of size winding, which is a property of a Hermitian operator O, the Hamiltonian H of the system, the temperature β, and the time t at which the operator $O = O(t)$ is evaluated in the Heisenberg picture. For simplicity, we assume that the Hilbert space of our system is that of n qubits (there is an analogous definition for fermions [11]). Let $\rho_\beta = e^{-\beta H} / \operatorname{tr} e^{-\beta H}$. Expand the operator $\rho_\beta^{1/2} O$ in the Pauli

basis as

$$\rho_\beta^{1/2} O = 2^{-n/2} \sum_P c_P P, \tag{1}$$

where the sum runs over all n-qubit Paulis [22]. Write $|P|$ for the size of an n-qubit Pauli operator, i.e., the number of qubits on which the operator acts nontrivially, e.g., $|X_1 Y_2 Z_5| = 3$. We define the *winding size distribution*:

$$q(l) := \sum_{|P|=l} c_P^2. \tag{2}$$

The winding size distribution should be contrasted with the more conventional size distribution, $\mathcal{P}(l)$, which is manifestly positive:

$$\mathcal{P}(l) := \sum_{|P|=l} |c_P|^2. \tag{3}$$

Note that the conventional size distribution and the winding size distribution coincide at infinite temperature $\beta = 0$, since $\rho_\beta^{1/2} O(t)$ is then Hermitian operator and thus $c_P \in \mathbb{R}$. However, for $\beta > 0$, c_P can have arbitrary phases. *Size winding*, in its perfect form, is an ansatz for the phase of c_P:

$$c_P = e^{i\alpha|P|/n} r_P. \quad r_P \in \mathbb{R}. \tag{4}$$

This equation says two things. (1) The phases of c_P only depend on the size $|P|$. There are many operators P of
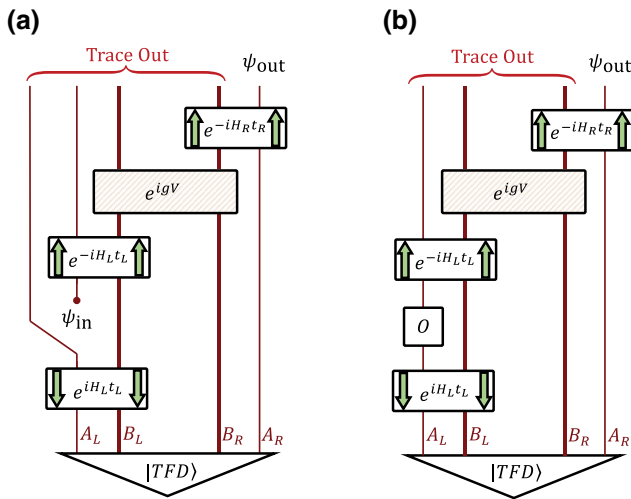
FIG. 4. The circuits considered in this paper, with $H_L = H_R^T$. Downward arrows indicate acting with the inverse of the time-evolution operator. In both protocols, the goal is to transmit information from the left to the right. (a) The *state-transfer* protocol calls for us to discard the left message qubits (A_L) and replace them with our message Ψ_{in}. The output state on the right then defines a channel applied to the input state. (b) The *operator-transfer* protocol calls for the operator O to be applied to A_L. Based on the choice of operator, the output state on the right is modified, similar to a perturbation-response experiment.

the same size, so this is already a nontrivial statement. (2) The phase dependence on size is linear. One subtlety of this condition is that r_P could be positive or negative; the

phase is thus allowed to take the form $\theta_P = \alpha|P| + \pi n(P)$, with $n(P) \in \mathbb{Z}$. The condition on the phases of the operator wave function given in Eq. (4) is fine grained and for a chaotic system seems challenging to check at first glance. However, a necessary and sufficient condition for perfect size winding is

$$q(l) = \mathcal{P}(l)e^{2i\alpha l/n}. \qquad (5)$$

Necessity follows immediately from the above definitions. To see that this condition is sufficient, note that $|q(\ell)| \le \mathcal{P}(l)$ with equality if and only if the phase of c_P depends only on $|P|$. Thus $c_P = r_P e^{i\theta(|P|)}$ for $r_P \in \mathbb{R}$. Plugging into Eq. (5), we obtain $\theta(|P|) = \alpha|P|$, which is exactly the size-winding condition. We use this criterion to show perfect winding for the SYK model in Appendix C 4.

What is the motivation for the size-winding ansatz? As we discuss in Ref. [4] and further review in Sec. III A, the traversable wormhole signal when we couple the two sides by e^{igV} is essentially the Fourier transform of the size-winding distribution [see Eq. (17)]:

$$\langle \text{TFD}| \, O_R(t)e^{igV}O_L(-t) \, |\text{TFD}\rangle = \sum_\ell q(\ell)e^{ig\ell}. \qquad (6)$$

An optimal teleportation protocol would seek to maximize the above signal. In general, the magnitude of the traversable wormhole signal satisfies

$$\left| \sum_\ell q(\ell)e^{ig\ell} \right| \le \sum_\ell P(\ell). \qquad (7)$$
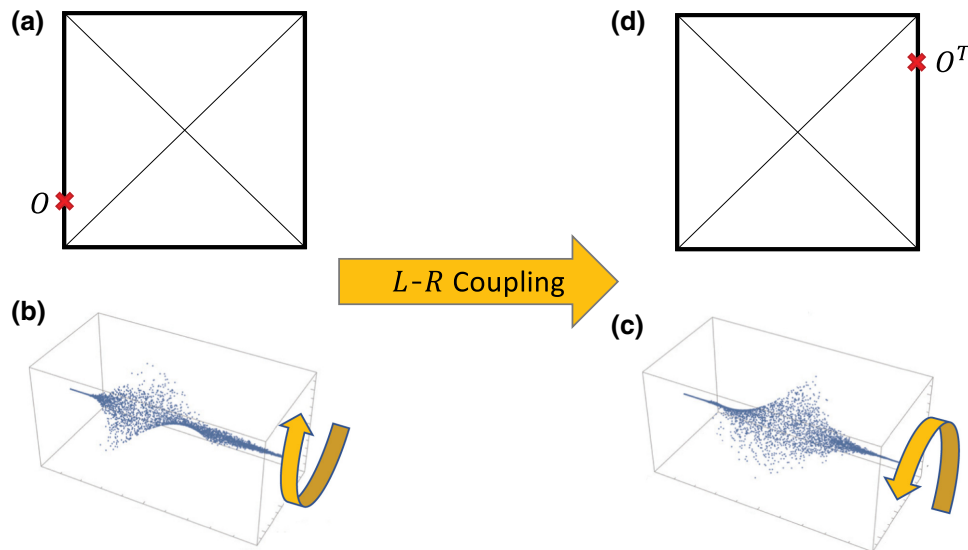

FIG. 5. Traversing the wormhole from the boundary point of view. (a) An operator O inserted at negative time t into the left boundary. (b) The (winding) size distribution of the thermal operator $O(t)\rho_\beta^{1/2}$, which is winding in the clockwise direction. (c) The size distribution after the application of *LR* coupling. The coupling applies a linear phase to the size distribution of the thermal operator in (b), unwinds it, and winds it in the opposite direction. In this way, we obtain a counterclockwise size distribution corresponding to the thermal operator $\rho_\beta^{1/2}O(t)$. (d) As we see in Ref. [4], winding in the opposite direction corresponds to the operator inserted on the other boundary at a positive time. Thus, the coupling maps the operator O on the left to operator O^T on the right.

Plugging in the size-winding ansatz, we see that this bound is saturated when $g = -2\alpha$. In other words, if we find a quantum system that exhibits perfect size winding, we are assured that optimal teleportation by size is possible.

We expect systems with a "clean" holographic dual to exhibit size winding. In this paper, we check this condition by a direct bulk calculation in nearly AdS$_2$ gravity. In systems without a clear holographic dual, the winding size distribution $q(l)$ will still typically obtain a complex phase. However, this phase may be a nonlinear function of l, or $|q(l)| < P(l)$. In these cases, we say that the system has imperfect winding. An example of such systems that we study in this paper is the ensemble of low-temperature random Hamiltonian systems (see Sec. II A). Imperfect winding sometimes can lead to low-quality transmission of information near the scrambling time. In other words, size winding can be viewed as a generalization of the traversable wormhole mechanism that applies to systems with and without a clear holographic dual.

II. EXAMPLE SYSTEMS

In this section, we study a number of paradigmatic quantum systems and analyze their ability to teleport with state-transfer or operator-transfer protocols. The simplest case, the case of infinite-temperature random unitary time evolution, is discussed in Ref. [4] and is not repeated here.

A. Random Hamiltonians

In this section, we present a detailed analysis of state and operator transfer when the Hamiltonian H is coming from the Gaussian unitary ensemble (GUE) or the Gaussian orthogonal ensemble (GOE). The GUE (GOE) means that each matrix element of the Hamiltonian matrix is an independent random variable coming from the complex (real) Gaussian distribution, with the extra constraint that H is Hermitian (symmetric). These ensembles are not expected to have proper gravitational dual but they can be analytically solved for all regimes of all relevant variables—in particular, at low temperatures. Nevertheless, we see that even random Hamiltonians have some features in common with the gravitational systems and exhibit imperfect size winding. The detailed analytical calculations are complicated and tedious, and mostly computerized. The relevant techniques are reported in Appendixes B and C 2.

1. High-temperature regime

The eigenvalue distribution of both the GUE and the GOE is the Wigner semicircle [23] and we assume that the distribution is normalized such that the edges of the semicircle are located at $\{-1, +1\}$. Such systems scramble "too fast" and at the time of the order of thermalization time. The (winding) size distribution $q_{l_0}(l)$ [defined in Eq. (2)] of

an operator with the original size of $l_0 \geq 0$ can be explicitly computed using the random-matrix-theory techniques (see Appendix C 2 b) and the result is a distribution with two branches (at $\beta = 0$):

$$q_{l_0}(l) = \delta_{l,l_0} \times f(it)^4 + \mathcal{N}(l) \times (1 - f(it)^4), \quad (8)$$

where $\mathcal{N}(l)$ is the normal distribution with mean $(3/4)n$ and standard deviation $\sqrt{2n}/3$, f is the Fourier transform of the semicircle distribution, $f(z) := 2I_1(z)/z$, and $I_1(z)$ is the modified Bessel function of the first kind and of order 1. Note that this is not similar to the growth pattern of local Hamiltonians, for which the operator size continuously flows to larger sizes (for the operator growth in random 2-local Brownian circuits, see, e.g., Fig. 9). Here, $q_{l_0=0}(l) = \delta_{l,l_0}$ and we observe that as time increases, $f(it)$ goes from 1 to 0, moving the size of the operator from a peak at l_0 to a peak at $l = 3n/4$. The distribution has two branches at all times, because the random Hamiltonian evolution either keeps a Pauli operator untouched or maps it to random Pauli strings.

Random matrix theory techniques are powerful enough to let us compute the precise average teleportation channel, even with the freedom of choosing the left and right times, t_L and t_R, independently (for the calculations, see Appendix C 2 and for a snapshot of the results, see Fig. 6).

2. Low-temperature regime and size winding

The winding size distribution q_l can be explicitly computed at low temperatures. Again, $q_{l_0}(l)$ has two branches at the initial size l_0 and $l = 3n/4$. The calculation techniques are explained in Eq. (C27) of Appendix C and here we report the final formula for the winding size distribution:

$$q_{l_0 \geq 1}(l) = \delta_{l,l_0} \frac{f(it - \beta/2)^2 f(it)^2}{f(-\beta)^2}$$
$$+ \mathcal{N}(l) \frac{[f(\beta/2)^2 - f(it - \beta/2)^2 f(it)^2]}{f(-\beta)^2}, \quad (9)$$

where $\mathcal{N}$ and f are defined above. It is easy to see that $f(it - \beta/2)$ becomes nonreal when t and β are both nonzero, giving a complex twist to q_{l_0}. This confirms the existence of some size winding for the GUE. Unlike the SYK model, the absolute value of size $|q(l)|$ is highly damped, indicating that the phase winding of individual coefficients is not coherent in this model. We call this "imperfect" size winding, which should be common in quantum systems on the general grounds of analyticity.

3. Low-temperature regime, state transfer, and operator transfer

Let us focus on the state-transfer protocols for GUE or GOE Hamiltonian systems. In Appendix C 2, we show that
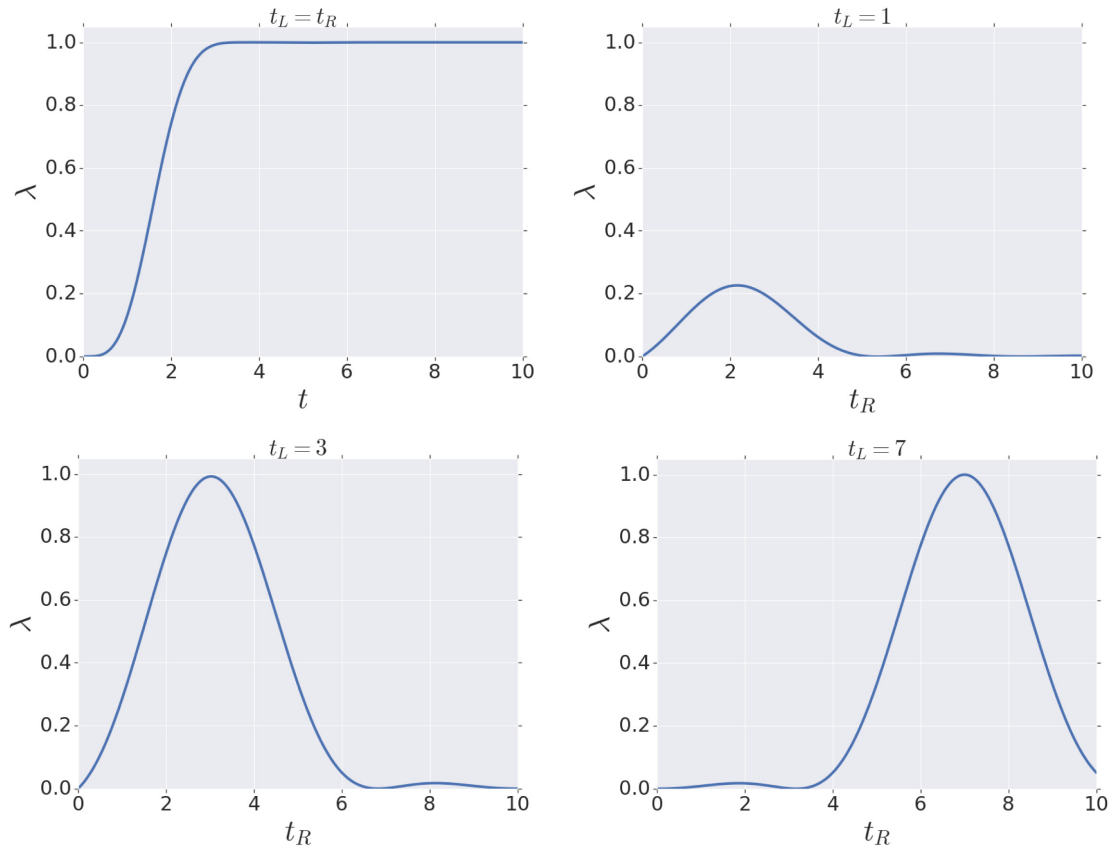
FIG. 6. Analytical results for the infinite-temperature state-transfer protocol for sending one qubit ($m = 1$), when the Hamiltonian is coming from the GOE and at $g = \pi$. The average channel always has the form of a depolarizing channel with parameter λ, conjugated by Pauli Y (see Eq. (3) in Ref. [4]). A small λ corresponds to a degraded signal, while $\lambda = 1$ indicates perfect transmission. Top left: the plot of λ when the sending time $-t_L$ is the same as the probing time t_R. Top right: the plot of λ as a function of the probing time t_R, when $-t_L = -1$. A weak signal comes out at $t_R \simeq 2$. Bottom left: the plot of λ as a function of the probing time t_R, when $-t_L = -3$. A strong signal is observed at $t_R = 3$. Bottom right: the plot of λ as a function of the probing time t_R, when $-t_L = -7$. After the scrambling time, the probed signal is maximized at $t_R = t_L$.

it still has the form of Eq. (3) of Ref. [4], with λ showing a strong dependence on sign(g) [24] (see Fig. 7). Note that the overall fidelity and the magnitude of the two-point function are still very small for the fidelity bounds in Eqs. (14) and (15) of Ref. [4] to be useful. Nevertheless, we see in Fig. 7 that there is a clear improvement of the signal for one sign of g. We believe that the $g \leftrightarrow -g$ asymmetry of the fidelity is partly sourced by size winding (proving this mathematically is the subject of future research). In fact, a close examination of the λ for these systems show that it gains contributions from the real part of two-point function $\langle e^{-igV} P_L(-t) e^{igV} P_R(t) \rangle$ as well as the three-point functions $\langle P''_R(t) e^{-igV} P'_L(-t) e^{igV} P_R(t) \rangle$ with $\{P, P', P''\} = \{X, Y, Z\}$. A clear sign($g$)-dependent signature in a two-point function is sufficient to produce a $g \leftrightarrow -g$ asymmetry in the fidelity, as seen in Fig. 7(a). This shows that although the bump in the fidelity is very suggestive of the signal traversing in a wormhole, one should be careful to attribute the bump to size winding alone (the situation is

less challenging in the operator-transfer protocols, which are directly related to the left-right two-point function).

Indeed, the state-transfer experiment above is not specifically designed to detect the physics of traversable wormholes (i.e., size winding) and it is only *weakly sensitive* to that phenomenon. This is not true when the size winding is near perfect, because in that case $|\tilde{q}_{l_0}(g)|$ is close to 1 and the bound given in Eq. (14) of Ref. [4] is saturated, predicting a specific value for the fidelity (which might be small).

To more directly observe the signals moving in traversable wormholes, one can use the operator-transfer protocol in Fig. 4 and select $O = e^{i\epsilon\phi}$. Then, the response of the right-hand-side density matrix attained by measuring the ϕ operator in the leading order in ϵ is the left-right commutator $\langle [e^{-igV} \phi_L(-t) e^{igV}, \phi_R(t)] \rangle$ (see Fig. 7). The response that one gets should have a sharp bump at low temperatures, which should be stronger for one sign of g. Moreover, the gravity should be able to send multiple
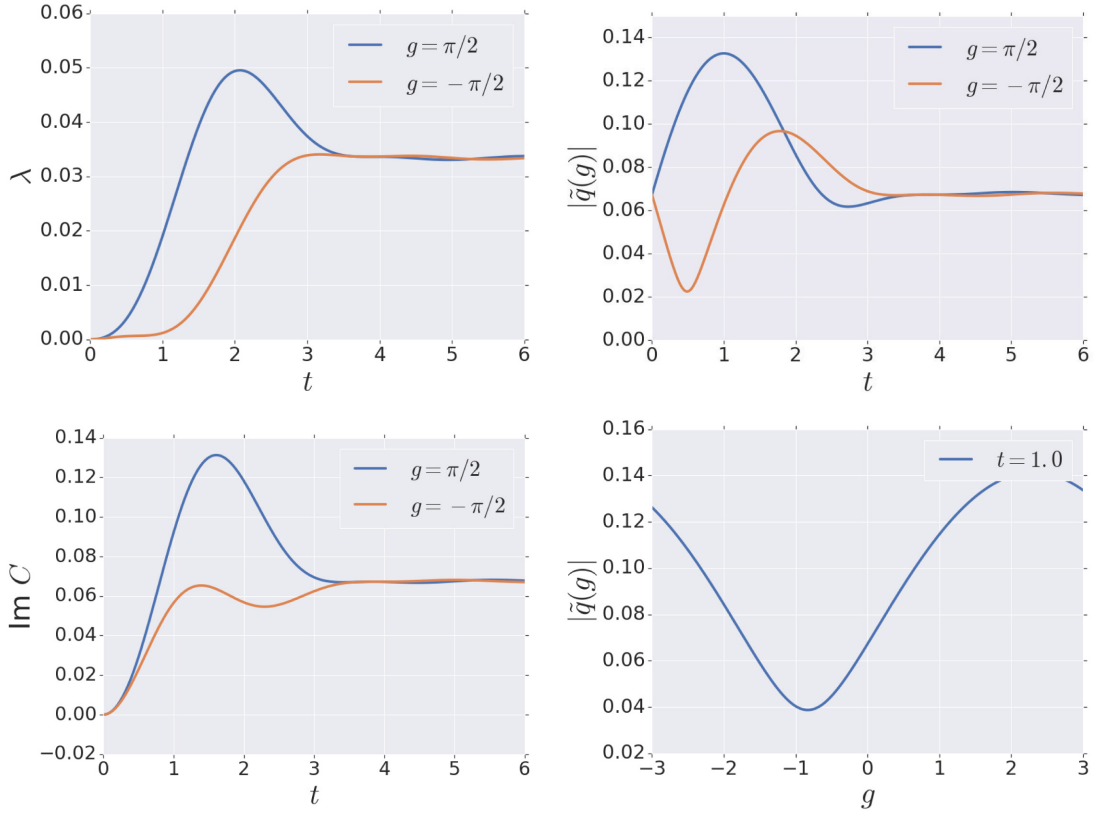
FIG. 7. A teleportation channel with a random Hamiltonian at $\beta = 20$. Top left: the GOE Hamiltonian depolarizing parameter λ. It clearly shows an improvement in the fidelity and quality of the channel for positive g. Top right: $|\tilde{q}(g)|$ for the GUE Hamiltonian [recall that $\tilde{q}(g) \approx e^{-ig} \langle T| P_R(t)e^{igV}P_L^T(-t) |T\rangle$; see Eq. (12) of Ref. [4]]. The phenomenon of size winding modifies the value of the two-point function $|\tilde{q}(g)|$ for early times in a sign(g)-dependent way. Bottom left: the imaginary part of $C = \langle e^{-igV}\phi_L(-t)e^{igV}\phi_R(t)\rangle$. Im C is the value of the commutator of left and right, an indicator of the causal signal. Bottom right: $|\tilde{q}(g)|$ as a function of g at $t = 1$. It shows a clear asymmetry around $g = 0$ at low temperatures.

operators; hence it should have a large capacity. Although this behavior is similar to what we expect from the fidelity of the teleportation protocols, it is much easier to interpret this phenomenon as a consequence of size winding in the operator-transfer experiment. This is particularly evident when we move away from completely nonlocal GUE-GOE Hamiltonian systems: for most k-local systems, the size distribution of the thermal state is narrow compared to n and $\langle e^{-igV}\phi_L(-t)e^{igV}\phi_R(t)\rangle \simeq e^{ig\langle V\rangle}\langle\phi_L(-t)e^{igV}\phi_R(t)\rangle$, as the coupling gives the same phase to same-sized operators. This shows that the commutator is directly related to $\tilde{q}_{l_0}(g)$ and is highly sensitive to size winding. In practice, one needs many runs of experiments to measure this type of signal, as ϵ is small.

B. Spin chains

Given knowledge about how the teleportation circuit in Fig. 4(a) works when the time evolution is modeled by random unitaries, we can deduce its behavior when the time evolution is a local random circuit or a that of a chaotic spin chain. Here, we primarily focus on local random circuits

[see Fig. 8(a)], as they have operator growth patterns that are similar to those of chaotic spin chains and are slightly easier to analyze. We only give an intuitive description of teleportation for such systems in this section and refer to Appendix C 1 for a rigorous argument.

Random local circuits can be constructed by considering a chain of qubits and applying randomizing unitaries between neighboring sites [see Fig. 8(a)]. We start by looking at the system at relatively early times. At that time scale, the spin chain looks like a stack of many random unitary blocks in parallel [see Fig. 8(b)] and therefore is capable of sending many qubits through the parallel application of the random unitary teleportation discussed earlier, i.e., one qubit per block (for the case of random unitary time evolution, see Ref. [4]). However, as time passes, the random blocks grow and recombine [see Fig. 8(c)], which reduces the total number of random blocks in the system, hence reducing the capacity of the channel [25]. This continues until the whole system is one large random scrambling block, which can teleport only one qubit.

Indeed, the protocol cannot be used too early, as the random local circuit needs some time in order to start to
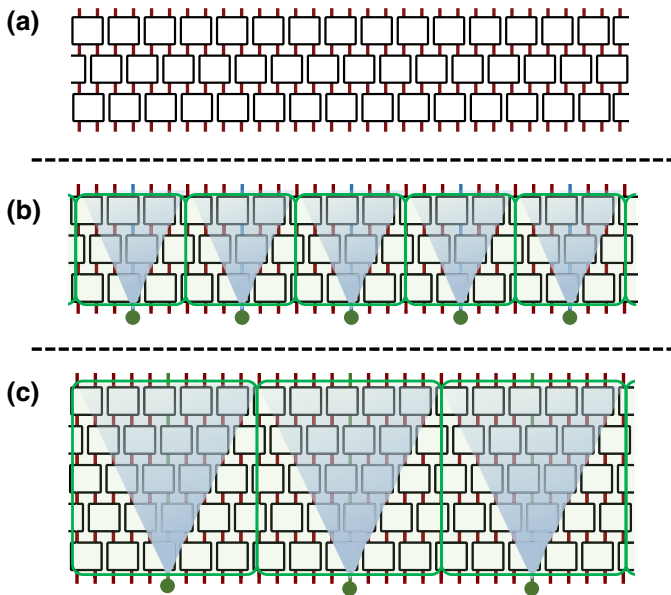
FIG. 8. (a) A snapshot of the time evolution of a one-dimensional random local circuit. (b) The circuit scrambles the degrees of freedom locally and, intuitively, it looks like a stack of parallel random unitaries (the green boxes), with the length scale given by the size of the light cone. Teleportation by size for random unitaries teaches us that we can use each individual random unitary as a resource teleporting exactly one qubit (teleporting qubits indicated by dark green circles, while the ZZ coupling acts on other qubits). (c) As time passes, the random boxes start to grow and recombine. Hence, the number of available boxes, and consequently the number of teleported qubits, will decrease.
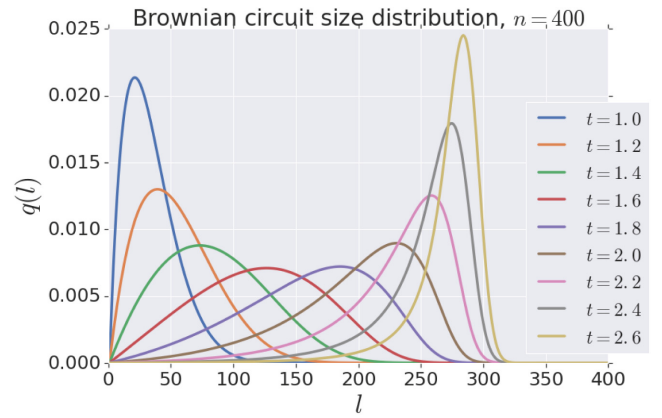

FIG. 9. An analytical evaluation of the size distribution of 2-local Brownian circuits on $n = 400$ qubits. The operator starts small and its evolved size is plotted for a different range of times. At $t = 1$, the operator size is still small. Then, it becomes wider until $t \simeq 1.6$ and starts to reconcentrate to the final value afterward. The final width is a function of n and the peak is sharper for larger n (this is because at late times the time-evolved Pauli looks like a random string of single-qubit Pauli operators.). However, the width of the size distribution at the intermediate times only weakly depends on n (for evidence, see Fig. 14).

scramble the system locally. The teleportation can be successful as long as (1) the total value of the g charge in each random block is equal to π and (2) the size of the block is large, such that the error term $\pi^2/(\text{block size})$ is small (see Appendix C 1). Note that g should be updated to $\pi/(\text{block size})$ in real time to satisfy point (1).

C. Nonlocal Brownian circuit models

Nonlocal Brownian circuits, in the context of gravity, have been proposed to model the black-hole dynamics as fast scramblers [26]. In this section, we study the operator growth in such systems and their capacity to teleport via teleportation by size. We mostly discuss an intuitive picture and refer the reader to Appendix C 3 for exact definitions and calculations.

Unlike the previous models that we have studied, i.e., random unitary time evolution, random GUE-GOE Hamiltonian evolution, and chaotic random circuits, this model has a proper operator growth pattern that mimics that of holographic systems such as the SYK model. On the other hand, we observe that this model lacks size winding, which severely limits its potential for holographic teleportation.

Here, we consider a 2-local Hamiltonian where all terms independently and rapidly change with time. These systems only exist at infinite temperature and can be completely analyzed using Itô calculus. This analysis indicates that the operator growth behaves as follows. (1) Operators start small, where the width of the distribution is also small. (2) Then, the average size of the operators, as well as their "width," grows and they stay proportional to each other for a while. (3) Lastly, the operators recombine to a Gaussian distribution peaked at $3/4n$, near the scrambling time (see Figs. 9 and 14).

As is clear in Fig. 9, the size distribution is *overdispersed* before the scrambling time, i.e., its standard deviation is large and comparable to its mean. This feature is not specific to this model and is generic in a variety of systems including the SYK model. Overdispersion is detrimental to operator transfer at early times for high-temperature systems. It will cause the two-point function $\tilde{q}_{l_0=1}(g)$ to have a norm much smaller than one, as the Fourier transform of a wide real function is highly damped. Therefore the operator-transfer protocol will not work properly in the intermediate times.

For the state-transfer protocols, overdispersion suggests that the actual fidelity cannot become very large. More precisely, consider sending one qubit. For some value of g, we need $\tilde{q}_{l_0=1}(g) \approx -1$ in order to have good fidelity. However, the large width of the distribution will significantly reduce the absolute value of $\tilde{q}_{l_0=1}(g)$; hence, even though $\tilde{q}_{l_0=1}(g)$ can be a negative number, it is highly damped. This shows that F_q [defined in Eq. (13) of Ref. [4]] is much

smaller than 1 and that F cannot be arbitrarily close to 1 as a consequence of Eq. (15) in Ref. [4]. Note that since $|\tilde{q}_{l_0=1}(g)|$ is small, the upper bound of Eq. (14) in Ref. [4] does not match F_q and we cannot read the exact fidelity from the size distribution [27].

In the next section, we argue that as a result of size winding, the size distribution $q_{l_0}(l)$ can get nonreal for low temperatures. Hence, despite the overdispersion, $|\tilde{q}(g)|$ can become large.

D. The SYK model

Using the elegant techniques developed by Qi and Streicher [11], we study size winding in the SYK model in Appendix C 4. For simplicity, we use the same notation, i.e., $P_{l_0=1}(l)$ and $q_{l_0=1}(l)$, for the size and winding size of the fermionic system, but keep in mind that for the fermions we use the product of Majoranas instead of Pauli operators to expand the time-evolved thermal fermion (see Ref. [11]). The size distribution starts concentrated at a fixed value and just before the scrambling time, it grows enough so that its width is comparable to n. In this time regime, we show that the winding size distribution $q_{l_0=1}(l)$ obtains a phase linear in l, while $|q_{l_0=1}(l)|$ remains the same as the conventional size, $P_{l_0=1}(l)$. Hence, all of the expansion coefficients in $q_{l_0=1}(l)$ should have a linear phase that only depends on l. More precisely, the equality $|q_{l_0=1}(l)| = P_{l_0=1}(l)$ shows that this phase is coherent; otherwise, the absolute value of $q_{l_0=1}(l)$ would be damped due to phase cancellations.

In Appendix C 4, we show that the number of windings per standard deviation of the size distribution is a constant and is equal to $\beta J/(\pi^2 q)$. Hence, as time passes, the size distribution gets exponentially wider and the rate of size winding gets exponentially smaller. This explains why one needs a larger g to make the wormhole traversable at earlier times and the task is easier as we get closer to the scrambling time. Of course, if one waits too for too long, the size distribution recombines at the final equilibration value ($n/2$ for fermions and $3n/4$ for qubits) and the operator transfer through size winding will not work.

The phenomenon of size winding has a natural interpretation in terms of the size-momentum relations [9,28], which we explain properly in Sec. III A. The size distribution is believed to be dual to the momentum in the bulk [29] and the exponential overdispersion of the size distribution is indicative of the boost symmetry of the bulk, which multiplies the momentum distribution by an exponential factor. We point out that by studying the quantity $q_{l_0}(l)$ instead of $P_{l_0}(l)$, we have access to some phase information that, loosely speaking, resembles the phase of a momentum wave function: its frequency determines the bulk location relative to the black-hole horizon (for a pictorial presentation, see Fig. 1 and for a more accurate interpretation, see Sec. III).

Note that the fermion or Pauli expansion coefficients of a certain size usually average to zero; hence $q_{l_0}(l)$ (or its better known Fourier transform, the two-point function) defined using the square of the fermion (or Pauli) is a natural quantity with which to observe this winding. The winding suggests some form of factorization of information on the boundary: the information about the details of the operator inserted in the bulk is encoded in the details of c_P coefficients defined in Eq. (1) (or the fermionic counterparts), while the position and momentum of the infalling signal are encoded in the phase of the winding size distribution and its absolute value, respectively.

Let us follow the wormhole teleportation more accurately at the time of interest, i.e., slightly before the scrambling time. At that time, the size distribution has expanded enough such that the average size is of order n, but possibly only a small fraction of n. The operator is highly boosted and the momentum of its corresponding quanta is growing approximately with $e^{2\pi t/\beta}$ [see Eq. (C50)], saturating the chaos bound. But since the number of windings per standard deviation of the size is constant and equal to $\beta J/(\pi^2 q)$, the size frequency is also decreasing by the same exponential factor, $e^{-2\pi t/\beta}$, indicating that the operator is getting very close to the horizon. However, the operator is winding, e.g., in the clockwise direction. The left-right coupling simply twists the operator by an extra phase proportional to g and the size. As described before, if g has the right value such that e^{igV} accurately reverses the winding direction, the operator from the left side of the horizon will be mapped to its right side.

As mentioned above, one needs a larger g in order to teleport the particle at a slightly earlier time. This can be seen from the gravitational picture as well: at earlier times, the particle is further from the horizon and a stronger negative-energy shock wave is needed to push it to the other side of the horizon.

III. THE HOLOGRAPHIC INTERPRETATION

In Sec. II, we describe size winding purely from the boundary point of view. We argue that perfect size winding implies a strong traversable wormhole signal. The goal of this section is to show that in the context of a holographic system such as SYK, one can check that the size-winding ansatz is satisfied using bulk methods. To do so, we recall the bulk interpretation of size. The growth of the size of an operator is a basic manifestation of chaos and is related to a particle falling toward a black-hole horizon [11,30,31]. In the context of low-temperature SYK, or nearly AdS$_2$ holography, the bulk interpretation of size is particularly sharp [9]. We review this discussion and elaborate on its applications to the traversable wormhole. Viewing size as a bulk-symmetry generator gives predictions for the wave function of the infalling particle that traverses the wormhole. We emphasize how the symmetry viewpoint makes

predictions about the entire size wave function and not just the average size.

One caveat is that the holographic description of size, as presently understood, only makes sense when there are a large number of light bulk fields. This requirement is naively in tension with sub-AdS locality. This would be an awkward state of affairs for our proposal, since presumably a quantum mechanical system with sub-AdS locality would be interesting to realize experimentally. Note, however, that in principle, the "size" concept could apply to a bulk theory with a number of fields $1 \ll k \ll N$ (in the bulk language, $N \sim 1/G_N$). Such a theory could, in principle, have sub-AdS locality. In practice, we are unaware of any quantum mechanical models with nearly AdS_2 duals that have genuine sub-AdS locality.

A. Size and momentum

In the context of the traversable wormhole, the particle crossing the negative-energy shock wave experiences a (null) translation. The shock wave can, therefore, be interpreted as the generator of this translation, otherwise known as (null) momentum. The shock wave is a direct consequence of the interaction between the two sides, which in the SYK model is simply the "size" operator. Thus, the size operator is simply related to null momentum [6,9].

A more precise argument [9,32] can also be given. Readers unfamiliar with nearly AdS_2 may jump to Sec. IV. Our starting point is the approximate symmetry generators

$$B = H_R - H_L, \quad E = H_L + H_R + \mu V - E_0. \quad (10)$$

Here, V is a sum of operators on both sides: $V = \sum_{i=1}^{k} O_i^L O_i^R$. In the SYK model, the simplest choice would be to take $O_i = \psi_i$, so that $V \propto i \sum \psi_L^j \psi_R^j$ is essentially the size operator [33]. The operators B and E, acting on states near the TFD, have semiclassical interpretations as the boost generator and the global energy generator (after we tune the value of μ so that the TFD is an approximate ground state of E; see Ref. [32]). We then choose the constant E_0 such that $E |\text{TFD}\rangle = 0$. It is also natural to consider the combinations

$$P_\pm = -\frac{1}{2}(E \pm B). \quad (11)$$

The action of these generators in the $NAdS_2$ space-time is depicted in Fig. 10. Note that $P_\pm < 0$ in quantum field theory on AdS_2. For our purposes, the important point is that $e^{ia^\pm P_\pm}$ generate a null shift as the particle leaves the pink region. Furthermore, by choosing the appropriate sign of $a^\pm$, we can shift the particle backward so that it leaves the horizon. Now note that

$$-P_+ = H_R + \mu V/2 + E_0/2, \quad -P_- = H_L + \mu V/2 + E_0/2. \quad (12)$$
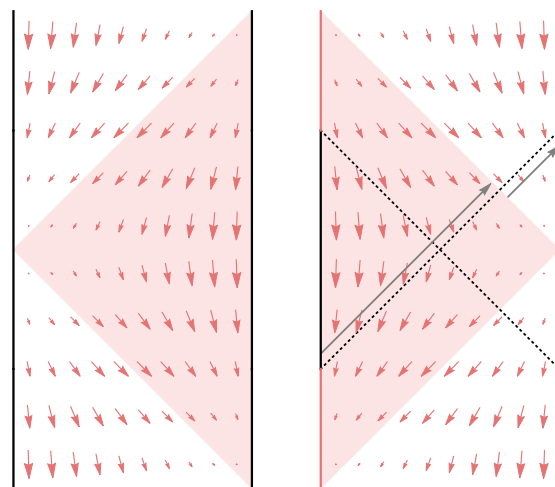

FIG. 10. The action of P_+ (left) and P_- (right) in AdS_2. These generators act by shifting Poincare time. The particle in the right diagram would experience a null shift when leaving the Poincare patch (shaded in pink). We also indicate in the right diagram the horizon (dotted black line) and the nearly AdS_2 boundaries (solid black segments). Note that with our conventions, physical future-directed quanta satisfy $P_+ < 0$, $P_- < 0$. Here, we are thinking of P_+ and P_- as being generated by operators at $t_L = t_R = 0$. By boosting these operators, we can obtain generators that act at $t_R = -t_L = t$. For large values of t, this gives us the null generators at the horizon.

The remarkable feature of this formula is that the action of P_+ (P_-) is exceedingly simple on the left (right) Hilbert space [34].

Consider a collection of Hermitian operators Γ_I, constructed by multiplying distinct Majorana fermions,

$$\Gamma_I \equiv \Gamma_{i_1 i_2 \ldots i_k} = 2^{-n/4} i^{\frac{k(k-1)}{2}} \psi_{i_1} \ldots \psi_{i_k}$$
$$1 \le i_1 < i_2 < \ldots < i_k \le n, \quad (13)$$

which forms an orthonormal basis for all operators acting on our Hilbert space $\text{tr}(\Gamma_I \Gamma_J) = \delta_{IJ}$. We define a temperature-dependent wave function for a given operator O:

$$\rho_\beta^{1/2} O = \sum_I c_I \Gamma_I. \quad (14)$$

We define the size-winding distribution as before:

$$q(s) := \sum_{|I|=s} c_I^2. \quad (15)$$

Just to familiarize ourselves with these definitions, let us check that

$$\langle \text{TFD}| O_R(t)O_L^T(-t) |\text{TFD}\rangle = \text{tr}\left(\rho^{1/2}O(t)\rho^{1/2}O(t)\right)$$
$$= \sum_I c_I(t)^2 = \sum_{s=0} q(s,t).$$
$$(16)$$

Note that this identity tells us that $\sum_s q(s,t)$ is independent of t. From now on, we assume that $O = O^T$ and drop the transpose (this is true if the initial operator is a product of an odd number of fermions). Now, the generalization of this formula in which we are interested is

$$\langle \text{TFD}| O_R(t)e^{i\mu V}O_L(-t) |\text{TFD}\rangle = \sum_I c_I^2(t)e^{i\mu|I|}$$
$$= \sum_s q(s)e^{i\mu s}, \quad (17)$$

so we see that the Fourier transform of the size-winding distribution q is related to the traversable wormhole signal. On the other hand, the Fourier transform of the conventionally defined size distribution $\mathcal{P}$ is

$$\langle \text{TFD}| O_R(t)e^{i\mu V}O_R(t) |\text{TFD}\rangle = \sum_s \mathcal{P}(s,t)e^{i\mu s}. \quad (18)$$

If we consider a more general correlator with $t_L \neq t_R$, we can obtain $q(s)$ by setting $t_L = -t_R = t$ and $\mathcal{P}(s)$ by analytically continuing $t_L = -t + i\pi, t_R = t$. We would like to compute both $q(s,t)$ and $\mathcal{P}(s,t)$ using a bulk calculation to verify the size-winding ansatz. To do so, consider

$$C(t) \equiv \langle \text{TFD}| O_R(t)e^{ia^- P_-}O_L(-t) |\text{TFD}\rangle$$
$$= \langle \text{TFD}| O_R \int dp_- |p_-\rangle \langle p_-| e^{ia^- P_-}O_L |\text{TFD}\rangle$$
$$= \int dp_- \psi_R^*(p_-)\psi_L(p_-)e^{ia^- p_-},$$
$$\psi_L(p_-) = \langle p_-| O_L |\text{TFD}\rangle. \quad (19)$$

Here, we are imagining that O creates a single-particle state of the quantum fields propagating in AdS_2. If the quantities on the left-hand side of Eqs. (17) and (19) were identical, we could then identify the size-winding distribution with a product of momentum wave functions $c_s^2 \sim \psi_R^*\psi_L$. While the quantities on the left-hand side of Eqs. (17) and (19) are not quite the same, they essentially differ only by a phase for our purposes. To understand this, let us use the boost

symmetry to rewrite the correlator as

$$C(t) = \langle \text{TFD}| O_R(0)e^{-iBt}e^{ia^- P_-}e^{iBt}O_L(0) |\text{TFD}\rangle \quad (20)$$
$$= e^{-ia^- E_0/2} \langle \text{TFD}| O_R(0)e^{-ia^-(\mu V(t,-t)+H_L)}$$
$$\times O_L(0) |\text{TFD}\rangle. \quad (21)$$

We see that the time dependence is coming from the boosted size operator $V(t,-t)$. More precisely, if we are interested in times $1 \ll t/\beta$ (but shorter than the scrambling time),

$$C(t) \approx e^{-ia^-(E_0/2+\langle H_L\rangle)} \langle \text{TFD}| O_R(0)e^{-ia^-(\mu V(t,-t))}$$
$$\times O_L(0) |\text{TFD}\rangle. \quad (22)$$

Using the definition of E_0, the global phase is just the average size of the TFD, $E_0/2 + \langle H_R\rangle = \mu \langle V\rangle /2$. Thus, we conclude that in this setup,

$$-P_- \approx \frac{1}{2}\mu\left(V - \langle V\rangle\right). \quad (23)$$

Here, V is the infinite-temperature size operator. At finite temperature, the relation is

$$\text{thermal size} = -2(\delta_\beta \mu)^{-1}P_-, \quad \delta_\beta \mu = \frac{2\alpha_S \mathcal{J}}{\Delta}(2\pi/\beta\mathcal{J})^2. \quad (24)$$

We emphasize that this equation (with the above approximations) should hold as an operator equation [35]. Comparing both sides of the equation, we can equate the wave functions:

$$q(s) \approx \psi_R^*(p_-)\psi_L(p_-). \quad (25)$$

The size-winding distribution is a sum over all operators with a given size $s = \langle V\rangle - 2p_-/\mu$. Therefore, we conclude that the bulk interpretation of the size-winding distribution is that it is a product of momentum-space wave functions. We expect the above formula to be valid in the low-temperature limit and for times $t \gg \beta$.

Now we would like to use the above ingredients to compute both $q(s)$ and $\mathcal{P}(s)$ in order to check the size-winding condition. First, we start by using the action of P_- on a conformal correlator:

$$\mathcal{C}_{\text{Sch}}(t_L, t_R) \propto \frac{1}{\left(4\cosh\frac{t_L+t_R}{2} - \tilde{g}e^{\frac{t_R-t_L}{2}}\right)^{2\Delta}}. \quad (26)$$

Now we can Fourier transform in $\tilde{g}$ to write

$$\mathcal{C}_{\text{Sch}} = e^{-2\Delta(t_L-t_R)}\int_0^\infty s^{2\Delta-1}\exp\left[-2is\left(e^{t_L} + e^{-t_R}\right)\right]e^{i\tilde{g}s}. \quad (27)$$

We define $\mathcal{C}$ by stripping off an irrelevant multiplicative constant $\mathcal{C} \propto C$ and setting $2\pi t/\beta \to t$ (to be restored by

dimensional analysis). Now, to compute the size-winding distribution, let us specialize to $t_L = -t_R, t_R = t + i\epsilon$. Then,

$$
\begin{aligned}
\mathcal{C}_{\text{Sch}}(-t, t) &= e^{-2\Delta t} \int_{-\infty}^{0} ds\, s^{2\Delta - 1} \\
&\quad \times \exp\left[-4se^{-t}(-i + \epsilon)\right] e^{i\tilde{g}s}, \\
\Rightarrow q(s, t) &\propto e^{-2\Delta t} s^{2\Delta - 1} \exp\left[-4se^{-t}(-i + \epsilon)\right]. \quad (28)
\end{aligned}
$$

On the other hand, to compute $\mathcal{P}(s, t)$, we set $t_L = -t + i\pi + i\epsilon', t_R = t + i\epsilon'$:

$$
\begin{aligned}
\mathcal{C}_{\text{Sch}}(-t + i\pi, t) &= (-e^{-2t})^{\Delta} \int_{-\infty}^{0} ds\, s^{2\Delta_\phi - 1} \\
&\quad \times \exp\left[-4se^{-t}\epsilon'\right] e^{i\tilde{g}s}, \\
\Rightarrow \mathcal{P}(s, t) &\propto e^{-2\Delta t} s^{2\Delta - 1} \exp\left[-4s\epsilon' e^{-t}\right]. \quad (29)
\end{aligned}
$$

Here, ϵ and ϵ' are ultraviolet (UV) regulators that make the two-point function at $t = 0$ finite. This is necessary to match with any system like SYK where the conformal symmetry emerges in the infrared (see, e.g., Ref. [9, Sec. 6.2] and Appendix D of this paper). By comparing the integrand of Eq. (29) with that in Eq. (28), we conclude that

$$
q(s, t) = \mathcal{P}(s, t) e^{i\alpha s}, \quad \alpha \propto -\epsilon e^{-t}. \quad (30)
$$

If we want to go beyond zeroth order in ϵe^{-t}, we have to assume that $\epsilon = \epsilon'$. This can be justified in the large-q SYK model (see Appendix D). As a further application of these formulas, we can compute the average size of a fermion. The integrand of Eq. (29) has an exponentially decaying factor $\exp\left(-4\epsilon(-p_-)/e^t\right)$ in $s \sim -p_-$, so we expect an average size $\propto e^t/\epsilon$. To be more precise, $\mathcal{C}(-t + i\pi, t)$ is a generating functional for size and restoring factors of $2\pi/\beta$:

$$
\begin{aligned}
\langle \text{thermal size} \rangle &= -2(\mu\delta_\beta)^{-1} \langle P_- \rangle = 2i(\mu\delta_\beta)^{-1} \partial_{\tilde{g}} \\
&\quad \times \log \mathcal{C}(-t + i\pi, t)|_{\tilde{g}=0} \\
&\propto \frac{\Delta^2}{\alpha_S \epsilon \mathcal{J}} (\beta \mathcal{J})^2 e^{2\pi t/\beta}. \quad (31)
\end{aligned}
$$

Setting $\epsilon \sim 1/\mathcal{J}$ as in Ref. [9] gives the correct answer for the average size in the regime $\beta \ll t \ll t_*$. Our formulas for $C(t)$ agree with the results of Ref. [6] in the probe limit, where gravitational back reaction is ignored. Indeed, after the scrambling time [36], the semiclassical approximation breaks down and the symmetry generators no longer are given by Eq. (10). From the boundary point of view, since our system is finite, the size of the operator cannot continue to grow exponentially but must saturate.

To summarize, we learn that the momentum-space wave function of a particle in AdS$_2$ is closely related to the size wave function of the operator. Using the momentum wave function, we verify that simple operators satisfy size winding at times $1 \ll t/\beta$ but smaller than the scrambling time $t \ll t_*$. The Fourier transform of the momentum wave function is the position wave function. "Position" here means the coordinate conjugate to P_-, which is Poincare "time" (see Fig. 10). On the edge of the pink region, this coordinate parametrizes a null shift. (This is just to say that the "position" conjugate to size is null or timelike; it is not a spacelike position.) The action of the two-sided coupling e^{igV} in the traversable wormhole protocol simply shifts the position of the particle, allowing the particle to potentially exit the black hole. The upshot is that in a holographic setting, size winding is related to the location of the particle, e.g., whether the particle is inside or outside of the black-hole horizon.

Let us remark on a minor but potentially confusing issue: whether size is related to P_+ or P_-. The answer is that when a particle is thrown in from the left side at early (negative) times, the size of the operator corresponding to the particle is related to P_- in our conventions. If we had instead thrown in the particle from the right side of the TFD, the size would be related to P_+. Of course, the final answers about the size wave function are left-right symmetric.

B. A modified bulk protocol

One disadvantage of the old protocol is that we must insert the signal at some particular time $t_L = -t$ on the left side. If t is too large, then the back-reaction destroys the effect. If t is too small, the signal does not make it across the wormhole (at least in the semiclassical limit). In this subsection, we discuss a modified protocol that should work even when t is small.

This protocol is also interesting from the bulk perspective, synthesizing Refs. [9,37]. Indeed, we describe how the instantaneous coupling acts like a null momentum generator on the particle. One could wonder whether there is a teleportation protocol that simply evolves with a symmetry generator.

To understand this new protocol, let us first remind the reader that the microscopic definition of the approximate global energy $E \sim H_L + H_R + \mu O_L O_R$ is somewhat ambiguous. In particular, the important fact is that we deform the usual Hamiltonian $H_L + H_R$ by some operators that are highly correlated in the TFD state. The simplest choice is to take $O_L O_R \sim \sum_{i=1}^{n} \psi_L^i \psi_R^i$. However, there are many other choices. For example, we could consider a sum over only half the fermions on the left and right. (The price we pay is that at a fixed temperature, using fewer fermions makes μ bigger, which means that the range of temperatures in which E can be interpreted as the global energy of AdS$_2$ would be more limited.) Another option is

to consider what happens when

$$O_L O_R \sim \sum_{i=1}^{n/2} \psi_L^{2i} \psi_L^{2i-1} \psi_R^{2i} \psi_R^{2i-1}. \qquad (32)$$

This might seem like a somewhat odd choice but note that it has the feature that we can group the Majorana fermions into qubits $Z_L^i = \psi_L^{2i} \psi_L^{2i-1}$. Now, with this choice of global Hamiltonian E, the Poincare generator is as follows:

$$-P_+ = H_R + \frac{\mu}{2} \sum_i Z_L^i Z_R^i. \qquad (33)$$

Now, instead of evolving with P_+, we may instead measure the operators Z_L^i, which projects the left qubits into the eigenstate $|z_1, z_2, \ldots\rangle$, and then evolve with

$$-\tilde{P}_+ = H_R + \frac{\mu}{2} \sum_i z_L^i Z_R^i. \qquad (34)$$

Note that this operator only acts on the right Hilbert space.

In fact, the procedure we have just described may be viewed as a "symmetry"-based derivation of the "state-dependent" Hamiltonian described in Ref. [37]. There, the state $e^{-\beta H} |z_1, z_2 \cdots\rangle$ is viewed as a one-sided state with an end-of-the-world (EoW) brane (see also Ref. [21]). Here, we are taking a two-sided view; we expect that the act of projecting onto a state inserts a high-energy shock (see Fig. 11). Note, however, that if we instead evolve with the two-sided operator P_+ (without the tilde), we do not inject this shock-wave or EoW brane.

1. Entanglement wedge of the right side and a subset of the left

As a side note, let us remark that one does not need access to the full left side in order for the protocol to work. As we have already remarked, with some caveats we can use a finite fraction of the fermions. A useful concept is the entanglement wedge of the right side combined with a subset of fermions on the left side. Roughly speaking, the entanglement wedge is the bulk space-time region where a probe operator could (in principle) be reconstructed [38–43].

Just to make the connection with the recent island discussions [21], we again consider a protocol where only a finite subset k of the n fermions on the left-hand side is used. This means that at time $t = 0$, we separate the k fermions that we use in the construction of $\tilde{P}_+$ from the $n - k$ fermions that we no longer use. We consider the leftover $(n - k)/2$ qubits on the left-hand side the "garbage."

A further motivation for studying the extremal surface is the following. As discussed in Ref. [6], a traversable wormhole can be thought of as a geometrization of the
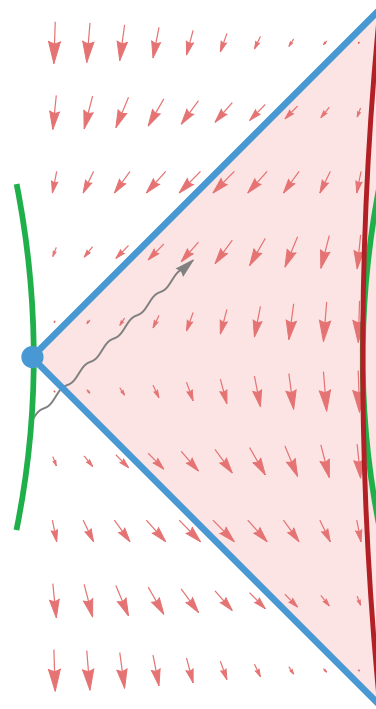

FIG. 11.   Teleportation at the end of the world. In this modified protocol, we insert a particle on the left at some time $t_L = -t$. Unlike the protocol in Ref. [5], t could be arbitrarily close to zero. The green trajectories show the standard evolution by $H_L + H_R$. A particle (wavy gray line) inserted on the left does not make it to the green boundary on the right. If we instead evolve with the symmetry generator $\tilde{P}_+$, the boundary particle on the right follows a trajectory of constant Poincare distance (dark red). The particle will then intersect the trajectory. Note that the point on the left indicated by the blue circle is a fixed point of the Poincare symmetry. When we evolve by P_+, the interpretation is that the left boundary is fixed at this space-time point. Alternatively, we may project onto an eigenbasis of the Pauli Z_i operators by performing a complete measurement on the left-hand side. This inserts an EoW brane [37].

Hayden-Preskill protocol. Alice throws her diary into one side of an old black hole. The black hole is sufficiently old that it is highly entangled with the Hawking quanta that have already been emitted. These Hawking quanta can be captured and collapsed into another black hole, which is entangled with the original black hole. Under favorable conditions, there will be a wormhole connecting the two black holes. The recovery of Alice's diary on the other side of the wormhole (by the teleportation experiment) may then be viewed as a protocol to recover information from the Hawking radiation.

The Hayden-Preskill protocol suggests that after waiting a scrambling time after Alice's diary is dropped in, one just needs to include a few bits from the original black hole (together with the earlier radiation) in order to recover what was in the diary. Rephrased in a modern language,

the Hayden-Preskill claim is that the entanglement wedge of the earlier radiation plus a few qubits of radiation from Alice's black hole contains enough of the interior of the black hole to include her diary. In our setup, this translates to the statement that the entanglement wedge of the right side plus a small fraction of the left will include a significant portion of the interior.

In Sec. III B, we adopt a two-sided view, but we could also adopt a one-sided view to make the connection with Ref. [21] explicit. Let us introduce some notation. We denote one-sided pure states

$$|B_{i\alpha}\rangle = e^{-\beta H/2} |i\rangle_k \otimes |\alpha\rangle_{n-k} \qquad (35)$$

$$|\tilde{B}_{i\alpha}\rangle = e^{-\beta H/2} O(t_L) |i\rangle_k \otimes |\alpha\rangle_{n-k}. \qquad (36)$$

Here, we arbitrarily divide the right side into k fermions and $n - k$ fermions; i and α label the computational-basis elements for the corresponding $k/2$ and $(n - k)/2$ qubits, respectively. This is a pure state for the right-side system with an EoW brane [37]. $|\tilde{B}\rangle$ is a perturbation of $|B\rangle$ with some particle behind the horizon. With these notations established, we return to our protocol. At $t = 0$, we have a two-sided state. After separating garbage qubits, we measure in the computational basis on the $k/2$ left qubits. This projects onto some definite state $|i\rangle_L$, so the combined system is in a state where the state of the $k/2$ left qubits factorizes from the garbage $\otimes$ right side. However, the state of (garbage $\otimes$ right side) does not tensor factorize:

$$\sum_\alpha |\alpha\rangle^L e^{-\beta H/2} |i\rangle^R |\alpha\rangle^R = \sum_\alpha |\alpha\rangle_{\text{garbage}} |\tilde{B}_{i\alpha}\rangle_R. \qquad (37)$$

We are left with a one-sided state, where the EoW brane states are entangled with an auxiliary system (the garbage, or the Hawking radiation).

If we model these brane states $|B_{i\alpha}\rangle$ using Jackiw-Teitelboim (JT) gravity + EoW branes as in the West Coast model [21], we may use their results to compute the entanglement wedge [21]. The garbage in our setup is

the analog of the "Hawking radiation" in the West Coast model. Indeed, we may compute the entanglement wedge of the garbage. If we discard too many qubits, an "island" will form and the signal we want to extract will be in the garbage. On the other hand, if the garbage only contains a small number of fermions, no island will form and the entanglement wedge of the right-hand side will contain the signal.

A potentially confusing point is that in the Hayden-Preskill setup, the garbage is the analog of the black hole (after a few Hawking quanta have escaped), whereas in the analogy with the West Coast model, the garbage plays the role of the radiation. There is no contradiction here. If we adopt the Hayden-Preskill interpretation of the traversable wormhole, the garbage is really the black hole; the connection with the West Coast model is just a device for computing the entanglement wedge. Just as in Ref. [6], we can say that the radiation system in the Hayden-Preskill setup has been processed and collapsed into its own black hole, which is why we interpret it as a black hole from the West Coast point of view.

The West Coast model has no propagating quantum fields, which is qualitatively dissimilar to SYK. A better model in the SYK context would be to study the entanglement wedge of JT gravity with free fermions in the bulk. The boundary of the entanglement wedge is determined by the QES prescription (in $1 + 1$ dimensions, the surface is just a point), which amounts to balancing the gradient of the dilaton ϕ against the entanglement entropy of m quantum fields in the bulk, where the m fields correspond to the m fermions we are including from the left. (For a review of the QES prescription in a similar context, see Refs. [10,44].)

To understand the contribution of the matter entropy, note that if we include a fraction of the fermions on the left-hand side, we can reconstruct the bulk fields dual to these fermions in a small wedge that is very close to the left boundary. More accurately, the state of any subset of fermionic qubits is basically unchanged over a
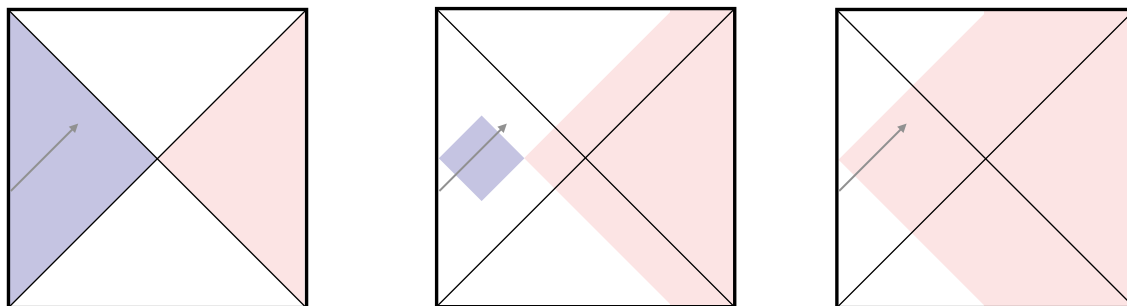

FIG. 12.   The entanglement wedge of the garbage is displayed in blue. The entanglement wedge of the right system plus m qubits on the left is displayed in pink. Left: when $m = 0$, the garbage contains the whole left side, so the quantum extremal surface is just the horizon. Center: as we decrease the size of the garbage, the island shrinks. Right: $m = n$. The entanglement wedge of the pink region extends all the way to the left boundary.

time scale of order approximately $1/J$ (when the interaction between becomes important). Therefore, using the Hamilton-Kabat-Lifschytz-Lowe prescription [45], we can reconstruct fields in a small wedge near the boundary. This means that the bulk-matter entropy S_m will gain a contribution from m fields in the subregion given by the union of a small interval near the boundary (the size of which is set by the UV cutoff $\epsilon \sim 1/J$) and the interval to the right of the quantum extremal surface.

If m is zero, then the extremal surface is just at the horizon, where the dilaton is minimized. However, the entanglement entropy of the m fields will shift the extremal surface further to the left (see Fig. 12). Some details are given in Appendix E, while more computations and a comparison with the SYK model will be reported in a future work [46].

IV. DISCUSSION AND OUTLOOK

We show, first in Ref. [4] and then in more detail in this paper, that there are two distinct mechanisms by which the traversable-wormhole-inspired quantum circuit can be used to transmit information:

(a) Mechanism 1: a generic information-teleportation phenomenon with no clear geometric interpretation, which works at high temperatures and times larger than the scrambling time
(b) Mechanism 2: a signal-transmission phenomenon that works via size winding and that occurs at low temperatures and near the scrambling time

While both mechanisms can transmit signals, only for mechanism 2 can the transmitted signal be interpreted as a particle traversing a holographic wormhole.

The two mechanisms above can be distinguished by measuring the winding size distribution, which, as we see in Eq. (12) of our companion paper [4], is the Fourier transform of the left-right two-point function (as a function of the coupling g). Therefore, the procedure for measuring the winding size distribution is not necessarily more difficult than the measurement of the original holographic teleportation signal—one could, in principle, reconstruct it from the left-right two-point function. Therefore, one can obtain something akin to a benchmark for "quantum gravity in the lab": any holographic teleportation protocol must necessarily display a signature of size winding.

In fact, we suggest something further: the existence of size winding alone could potentially provide a geometrical picture for teleportation. One can interpret the winding size as a momentum wave function of a one-dimensional particle. Indeed, in the low-temperature SYK model (where the holographic dual is understood), we observe that the winding size distribution is dual to the (null) momentum wave function of the infalling particle. Yet, even if we

are not aware of the existence of a bulk dual, we could heuristically define the winding size distribution to be the wave function of some one-dimensional particle, thereby obtaining a geometric picture. We leave this as an avenue for further study.

Finally, let us speculate on two other related benchmarks that could be used for "quantum gravity in the lab."

The first benchmark is the Lyapunov exponent of the out-of-time-ordered commutator [47–50], which determines the exponential rate of growth of the average size. Since this quantity only depends on the size distribution, it is not immediately sensitive to the phases of the operator wave function and it could be considered complementary to size winding.

A second related benchmark could be to verify the QES formula for the entropy of a subsystem by measuring the entropy and comparing with the holographic prediction. In practice, it may be easier to measure various Renyi entropies (using the replica trick) than measuring the von Neumann entropy. Moreover, the Renyi entropies can also be computed using a more sophisticated bulk calculation. Although at first glance this benchmark seems very different from the traversable-wormhole experiment, the two are in fact closely connected. As described in Sec. III B 1, the QES associated to the joint system of one side and a few qubits on the other must necessarily encompass the infalling particle within the black hole for the traversable-wormhole protocol to work.

In summary, we see that holographic traversable wormholes provide a promising model system in which to study "quantum gravity in the lab."

is supported by the Walter Burke Institute for Theoretical Physics and IQIM at Caltech. The work of G.S. was performed before joining Amazon Web Services.

Note added.— Recently, we learned of an independent investigation of the role of operator spreading in wormhole-inspired teleportation protocols by Schuster *et al.* [51].

APPENDIX A: PRELIMINARIES ON PAULI OPERATORS

In this appendix, we review the algebra of n-qubit Pauli operators and recall some useful identities. Consider the Hilbert space $(\mathbb{C}^2)^{\otimes n}$ of an n-qubit system. For any integer vector $\mathbf{v} = (\mathbf{p}, \mathbf{q}) \in \mathbb{Z}^{2n}$, we can define a corresponding *Pauli operator* (also known as a *Weyl operator*) by

$$P_\mathbf{v} = i^{-\mathbf{p}\cdot\mathbf{q}} Z^{p_1} X^{q_1} \otimes \cdots \otimes Z^{p_n} X^{q_n}. \quad (A1)$$

The Pauli operators $P_\mathbf{v}$ for $\mathbf{v} \in \{0,1\}^{2n}$ form a basis of the space of n-qubit operators. However, we caution that $P_\mathbf{v}$ depends on $\mathbf{v}$ modulo 4 and is well-defined modulo 2 only up to a sign. Namely,

$$P_{\mathbf{v}+2\mathbf{w}} = (-1)^{[\mathbf{v},\mathbf{w}]} P_\mathbf{v}, \quad (A2)$$

where $[\cdot,\cdot]$ is the "symplectic form," defined by $[(\mathbf{p},\mathbf{q}),(\mathbf{p}',\mathbf{q}')] = \mathbf{p}\cdot\mathbf{q}' - \mathbf{q}\cdot\mathbf{p}'$. Using this form, the commutation relation of the Pauli operators can be succinctly written as

$$P_\mathbf{v} P_\mathbf{w} = (-1)^{[\mathbf{v},\mathbf{w}]} P_\mathbf{w} P_\mathbf{v} \quad (A3)$$

and multiplication is given by

$$P_\mathbf{v} P_\mathbf{w} = i^{[\mathbf{v},\mathbf{w}]} P_{\mathbf{v}+\mathbf{w}}, \quad (A4)$$

where the addition $\mathbf{v} + \mathbf{w}$ in $P_{\mathbf{v}+\mathbf{w}}$ must be carried out modulo 4 and can only be reduced to the range $\{0,1\}$ by carefully applying Eq. (A2). Finally, we note that the transpose of a Pauli operator is given by

$$P_\mathbf{v}^T = (-1)^{\mathbf{p}\cdot\mathbf{q}} P_\mathbf{v}, \quad (A5)$$

since transposing only impacts the Y operators.

With these facts in mind, let us momentarily discuss the size of Pauli operators. The *size* of a Pauli operator $P_\mathbf{v}$, which we denote by $|P_\mathbf{v}| = |\mathbf{v}|$, is defined as the number of single-qubit Paulis in Eq. (A1) that are not proportional to the identity operator. If $\mathbf{v} \in \{0,1\}^{2n}$, then this can be calculated as $\mathbf{p}\cdot\mathbf{p} + \mathbf{q}\cdot\mathbf{q} - \mathbf{p}\cdot\mathbf{q}$, where the last term ensures that we do not double count Y operators. Using the above properties, we arrive at an identity that holds for all $\mathbf{v} \in \mathbb{Z}^{2n}$ and is frequently used:

$$Y^{\otimes n} P_\mathbf{v}^T Y^{\otimes n} = (-1)^{\mathbf{p}\cdot\mathbf{p}+\mathbf{q}\cdot\mathbf{q}} P_\mathbf{v}^T = (-1)^{|P_\mathbf{v}|} P_\mathbf{v}. \quad (A6)$$

APPENDIX B: PRELIMINARIES ON HAAR AVERAGES

In this appendix. we recall how to compute averages of the form $\mathbb{E}[\mathrm{Tr}[U^{\otimes r} A U^{\dagger,\otimes r} B]]$ where U is a random unitary $d \times d$ matrix chosen from the Haar measure. Any average over the unitary group that involves the same number r of matrix elements of U (or U^T) as of $U^\dagger$ (or $\bar{U}$) can be cast in this form for a suitable choice of A and B.

We first introduce some notation. Consider the permutation group S_r of r elements. For any Hilbert space $\mathcal{H}$, the permutation group S_r acts naturally on $\mathcal{H}^{\otimes r}$ by permuting the r replicas, i.e.,

$$R_\pi |\psi_1\rangle |\psi_2\rangle \cdots |\psi_r\rangle$$
$$= |\psi_{\pi^{-1}(1)}\rangle \otimes |\psi_{\pi^{-1}(2)}\rangle \otimes \cdots \otimes |\psi_{\pi^{-1}(t)}\rangle, \quad (B1)$$

where $|\psi_i\rangle \in \mathcal{H}$. If $\mathcal{H} = (\mathbb{C}^2)^{\otimes n}$ is the Hilbert space of n qubits, then R_π is a tensor power operator with respect to the n qubits and their replicas:

$$R_\pi = r_\pi^{\otimes n}, \quad \text{where } r_\pi |j_1, j_2, \ldots, j_r\rangle$$
$$= |j_{\pi^{-1}(1)}, j_{\pi^{-1}(2)} \cdots j_{\pi^{-1}(r)}\rangle \text{ and } j_k \in \{0,1\}. \quad (B2)$$

Now consider an arbitrary rth moment of the form

$$\mathbb{E}[U^{\otimes r} A U^{\dagger,\otimes r}], \quad (B3)$$

where U is chosen from the Haar measure on $\mathrm{U}(d)$ and A is an arbitrary operator on $(\mathbb{C}^d)^{\otimes r}$. Since Eq. (B3) commutes with all $U^{\otimes r}$ for $U \in \mathrm{U}(d)$, Schur-Weyl duality implies that it is a linear combination of the operators R_π for $\pi \in S_r$. For example,

$$\mathbb{E}[UAU^\dagger] = \mathrm{Tr}[A]\frac{I}{d}, \quad (B4)$$

since for $r = 1$ there is only the identity permutation. Similarly,

$$\mathbb{E}[U^{\otimes 2} A U^{\dagger,\otimes 2}] = \frac{d\,\mathrm{Tr}[A] - \mathrm{Tr}[AF]}{d(d^2-1)} I$$
$$+ \frac{d\,\mathrm{Tr}[AF] - \mathrm{Tr}[A]}{d(d^2-1)} F, \quad (B5)$$

where $F = R_{(12)}$ denotes the flip or swap operator that permutes the two replicas.

Higher moments can be conveniently calculated using the Weingarten calculus developed in Ref. [52]. To state the result, define the *length* $\ell(\pi)$ of a permutation $\pi \in S_r$ as the number of disjoint cycles in π (including fixed points). Then $|\pi| := r - \ell(\pi)$ is the minimum number of transpositions needed to write π and it is easy to see that $\mathrm{dist}(\pi,\sigma) := |\pi\sigma^{-1}|$ defines a metric on S_r. Now,

the results of Refs. [52,53] imply the following general formula for an rth moment:

$$\mathbb{E}[U^{\otimes r}AU^{\dagger,\otimes r}] = \sum_{\sigma,\tau \in S_r} \text{Wg}(\sigma\tau,d)\,\text{Tr}[AR_\tau]\,R_\sigma, \quad \text{(B6)}$$

where $Wg(\pi,d)$ is the *Weingarten function*. We do not define the Weingarten function here but only state its limit as $d \to \infty$:

$$d^{r+|\pi|}\,\text{Wg}(\pi,d) \to \text{Moeb}(\pi), \quad \text{(B7)}$$

where Moeb is the *Möbius function*, defined using the Catalan numbers $c_n = 2n!/(n!(n+1)!)$ as

$$\text{Moeb}(\pi) = \prod_{i=1}^{\ell(\pi)}(-1)^{|C_i|-1}c_{|C_i|-1} = (-1)^{|\pi|}\prod_{i=1}^{\ell(\pi)}c_{|C_i|-1}, \quad \text{(B8)}$$

in which $\{C_1,\ldots,C_{\ell(\pi)}\}$ is the cycle decomposition of the permutation π. Clearly, Eq. (B6) implies that

$$\mathbb{E}[\text{Tr}[U^{\otimes r}AU^{\dagger,\otimes r}B]] = \sum_{\sigma,\tau \in S_r} \text{Wg}(\sigma\tau,d)\,\text{Tr}[AR_\tau]\,\text{Tr}[BR_\sigma]. \quad \text{(B9)}$$

In most cases of interest for us, the matrices A and B in Eq. (B9) are close to tensor-product operators of the form $A = \otimes_{i=1}^n a_i$, $B = \otimes_{i=1}^n b_i,$. In this case, $\text{tr}[AR_\sigma] = \prod_{i=1}^n \text{tr}[a_ir_\sigma]$ and $\text{tr}[BR_\sigma] = \prod_{i=1}^n \text{tr}[b_ir_\sigma]$, which are easy to calculate.

APPENDIX C: EXAMPLES

1. Chaotic spin chains and random local circuits

In this appendix, we revisit the random-local-circuit discussion of Sec. II B in a more quantitative way.

As stated before, chaotic spin chains and random local circuits provide prime examples for the phenomenon of high-temperature state transfer, which could be experimentally realized with the current technology. Again, we primarily discuss the local-random-circuit models and point out that chaotic spin chains should behave similarly.

Consider a one-dimensional chaotic spin chain (higher-dimensional extensions are straightforward), where the A qubits (message qubits) are spread among the B qubits (carrier qubits) such that the distance of any two A qubits is larger than the $2v_Bt$, where v_B is the butterfly velocity and t is the time of the evolution. We assume that the random-circuit evolution (or the chaotic Hamiltonian evolution) turns a Pauli operator into a collection of random strings on its light cone (note that this should be exactly true for random-circuit models). Now, we discuss the size distribution. Start with operator P_A at $t = 0$, with the initial size $l_0 = |P_A|$. At later times, each nonidentity single

Pauli operator in P_A expands to a Pauli string of average size equal to $2 \times 3v_Bt/4$ (which is $3/4$ of the light-cone size $2v_Bt$). If $v_Bt \gg 1$ such that the variance of the size is negligible, we have

$$q_{l_0}(l) = \delta(l, l_0 \times 3v_Bt/2) \quad \text{(C1)}$$

[see Fig. 2(b)]. This shows that (for the definition of $\tilde{q}_{l_0}(g)$, see Eq. (12) of Ref. [4])

$$\tilde{q}_{l_0}(g) = e^{-il_0(4g/3)3v_Bt/2n} = e^{-il_0(g/n)2v_Bt}. \quad \text{(C2)}$$

As long as $(g/n)2v_Bt$, i.e., the total g charge on the light cone is an odd multiple of π, the norm of $\tilde{q}_{l_0}(g)$ is equal to one and it has an alternating sign as a function of l_0. Hence, this system can teleport all of the qubits in A_L with high fidelity according to Eq. (14) of Ref. [4]. We point out that the standard deviation of the size distribution is proportional to $\sqrt{l_0v_Bt}$, which should be much smaller than v_Bt, the distance between peaks in the size distribution [see Fig. 2(b)]. Therefore, the m-qubit fidelity is large only if $m \ll \sqrt{v_Bt}$.

2. Random nonlocal Hamiltonian in the GUE or GOE

Now, we focus on the actual Hamiltonian evaluations. We start with nonlocal completely random Hamiltonians. The benefit of using such systems is that we have complete analytical control over the calculations and one can easily go to the infinite system size and arbitrary parameters. The calculations are usually tedious, computerized, and use the techniques described in Appendix B. In Appendix C 2 a, we compute the state-transfer average output state as well as some two-point function. These quantities are generically complex and we only report the final results. The size distribution, which is calculated in Appendix C 2 b, is more manageable and we spend more time explaining the details of its calculations. Therefore, we refer the reader interested to learn the techniques of our calculations to Appendix C 2 b.

a. Average evolution with GUE or GOE Hamiltonians

Here, we report the formulas for the infinite- and finite-temperature GOE setup. We believe that there is no significant difference between the GUE and the GOE, except that for the GOE we have the luxury of having $H_L = H_R = H$. Again, we assume that there are n qubits on each side, that the coupling acts on all n of the qubits, and there is only one qubit to send ($m = 1$) [54].

Let us relax the condition of acting on the left and the right at the same time and assume that the left qubit is inserted at time $-t_L$ and the observation time is $+t_R$. The one-qubit teleportation channel is given by

$$\Psi_{S_L} \to [1 - \lambda(\beta, t_L, t_R)]\tau + \lambda(\beta, t_L, t_R) Y \Psi Y = Y \Delta_{\lambda(\beta, t_L, t_R)}(\Psi_{S_L}) Y, \tag{C3}$$

where we explicitly relax the condition of acting by the same times on the left and right and $\lambda(\beta, t_L, t_R)$ is the parameter of the depolarizing channel. In the limit as $n \to \infty$, $\lambda(\beta, t_L, t_R)$ is given by the following formula:

$$\lambda(\beta, t_L, t_r) = \mathrm{Re}\left[\frac{1}{2}(1 - e^{ig})f(-\beta/2 + i(t_R - t_L))f(i(t_R - t_L))f(-\beta/2)) + f(it_L)f(it_R)f(-\beta/2 + it_L)\right.$$

$$\times \left(\frac{1}{2}(1 - e^{ig})f(-\beta/2 + it_R) + (1 - e^{ig})f(it_L)f(it_R)f(-\beta/2 - it_L)\right.$$

$$\left.\left. - (1 - e^{ig})f(it_L)f(-\beta/2 + i(t_R - t_L)) - (1 - \cos(g))f(it_R)f(-\beta/2)\right)\right]/f(-\beta). \tag{C4}$$

As in the main text, $f(z) = 2 I_1(z)/z$ is the modified Bessel function of the first kind of order one. This is a relatively complicated formula but it is valid for all g, β, t_L, and t_R and it completely characterizes the teleportation channel through Eq. (C3). As one decreases n, then the first corrections to the above formula are obtained by the following substitutions of the g-dependent coefficients:

for finite n : $(1 - e^{ig}) \to \cos(g/n)^n \left[\cos(n/k)^n - e^{ig}\right]$,
$$\tag{C5}$$

and $(1 - \cos(g)) \to \cos(g/n)^n$
$$\times \left[\cos(g/n)^n - \cos(g)\right]. \tag{C6}$$

For very small n, e.g., $n = 6$ or $n = 7$, there are more corrections due to (1) the distribution of eigenvalues starting to deviate from the semicircle distribution and (2) the details of the eigenvalue statistics becoming relevant, as the separation between the time scale dictated by the inverse eigenvalue spacing and the time scale of interest, $t = O(1)$, gets less significant.

In the limit as $n \to \infty$, we can focus on to the infinite-temperature limit, $\lambda(t_L, t_R) := \lambda(\beta = 0, t_L, t_R)$:

$$\lambda(t_L, t_R) = \frac{1 - \cos(g)}{2}$$
$$\times \left[f(-it_R + it_L)^2 + 2f(it_L)^4 f(it_R)^2\right.$$
$$- f(it_L)^2 f(it_R)^2 - 2f(it_L)^3$$
$$\left.\times f(it_R)f(-it_R + it_L)\right], \tag{C7}$$

which, for $t_L = t_R$, simplifies to

$$\lambda(t) = \frac{1 - \cos(g)}{2}\left[1 + 2f(it)^6 - 3f(it)^4\right]. \tag{C8}$$

One can see that the same time-teleportation signal $\lambda(t, t)$ starts from 0 and plateaus at the value of $(1 - \cos(g))/2$, which is the same as the random unitary result (see Fig. 13). The plateau starts at time around $t = 2.7$, which is around the same time as the scrambling time or the thermalization time (which are both more or less the same for GOE nonlocal Hamiltonians).

It is interesting to look at the problem $t_L \neq t_R$. Indeed, we can fix the time at which we send the signal (t_L fixed) and vary the observation time t_R (see Fig. 6). If one sends the signal before the scrambling time ($t_L \lesssim 3$), the signal is weaker but still comes out at near scrambling time. However, for times larger than the scrambling time, the signal comes out at $t_R = t_L$.

We also report the results of the two-point function calculations:

(a) *Two-point function calculations I*. We can compute the following two-point function for GUE-GOE Hamiltonians:
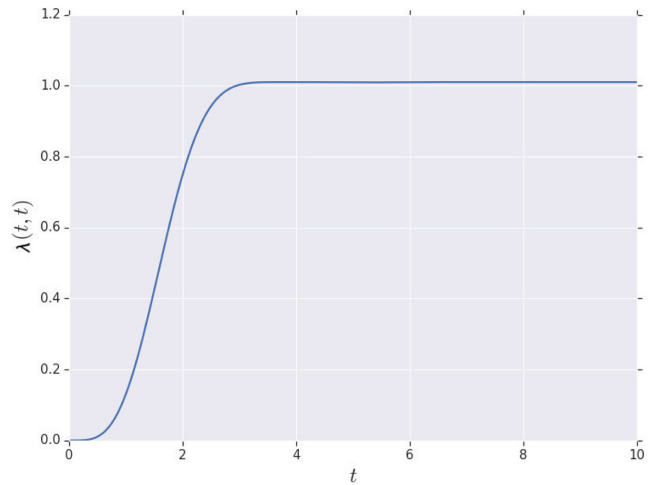

FIG. 13. A plot of the teleportation signal $\lambda(t, t)$ as defined in Eq. (C3), for a Hamiltonian coming from the GOE. This is plotted for $g = \pi$.

$$\langle T| P_R(t)e^{igV}P_L(-t) |T\rangle, \tag{C9}$$

in the limit of very large system size $n \to \infty$ and with the assumption that P is a single-qubit Pauli. This can be evaluated using Eq. (12) of Ref. [4] and the result that we derive in the next subsection [Eq. (C27)] to give

$$\frac{e^{ig}f\,(it-\beta/2)^2f\,(-it)^2 + \left[f\,(-\beta/2)^2 - f\,(it-\beta/2)^2f\,(-it)^2\right]}{f\,(-\beta)}. \tag{C10}$$

(b) *Two-point function calculations II*. We analyze a different two-point function:

$$\langle T| e^{-igV}P_R(t_R)e^{igV}P_L(-t_L) |T\rangle, \tag{C11}$$

for the GOE. For most k-local systems, the size distribution of the thermal state has a small variance and therefore the thermofield double state is close to being an eigenvalue of e^{igV}. This means that Eq. (C11) is simply proportional to the simpler two-point function given in Eq. (C9). This is not true for nonlocal random Hamiltonians, as their thermal state has two branches, one at the identity matrix and one a narrow Gaussian at $3n/4$. Hence, it is not possible to easily infer Eq. (C11) from Eq. (C9). With direct calculations, Eq. (C11) evaluates to

$$\frac{1}{f\,(-\beta)}\Bigg[2f\,(-\beta/2 + it_L)f\,(-it_L)f\,(it_R)f\,(-it_R)f\,(-\beta/2) \tag{C12}$$

$$-f\,(-\beta/2 - it_R + it_L)f\,(-\beta/2)f\,(+it_R - it_L) \tag{C13}$$

$$-f\,(-\beta/2 + it_L)f\,(-it_L)f\,(-\beta/2 + it_R)f\,(-it_R) \tag{C14}$$

$$+f\,(-\beta/2 - it_R + it_L)f\,(-\beta/2 + it_R - it_L) \tag{C15}$$

$$-e^{ig}f\,(-\beta/2 + it_L)f\,(-it_L)f\,(+it_R)f\,(-it_R)f\,(-\beta/2) \tag{C16}$$

$$+e^{ig}f\,(-\beta/2 + it_L)f\,(-it_L)f\,(-\beta/2 + it_R)f\,(-it_R) \tag{C17}$$

$$-e^{-ig}f\,(-\beta/2 + it_L)f\,(-it_L)f\,(+it_R)f\,(-it_R)f\,(-\beta/2) \tag{C18}$$

$$+e^{-ig}f\,(-\beta/2 - it_R + it_L)f\,(-\beta/2)f\,(+it_R - it_L)\Bigg]. \tag{C19}$$

Again, the proof of this formula requires lengthy computerized calculations involving Brauer-algebra contractions.

b. Size distribution

In this section, we present a more detailed derivation of the size distribution for the case of random Hamiltonian time evolution. Let us momentarily focus on the GUE; near the end, we mention the required modifications for GOE. We start with a calculation of the following form:

$$s(\alpha, \beta, \mathbf{u}, \mathbf{v}) = \frac{1}{d^2}\mathbb{E}_{H\sim\mathrm{GUE}}\big(\mathrm{tr}\left[e^{\alpha H} P_\mathbf{u} e^{\beta H} P_\mathbf{v}\right]\big)^2. \tag{C20}$$

We can easily see that the size distribution of $\rho_\beta^{1/2}e^{itH} = e^{itH - \beta/2H}$ can be read from the s function by proper substitution of its parameters.

We can diagonalize H as $H = UDU^\dagger$, where U is from the Haar measure on the unitary group; hence the name "Gaussian unitary ensemble." One can check that the eigenvalues of the diagonal matrix D have a semicircle distribution centered at 0 with radius 1. In the large-n limit, the details of the semicircle distribution would be unimportant for the times of $O(1)$ for which we study the problem and it can be assumed to be a smooth semicircle. The detailed eigenvalue distribution only manifests itself at exponential time and is a subject of important investigations in the study of

holographic dualities (see, e.g., Refs. [55,56]). In drawings, Eq. (C20) is

$$\frac{1}{d^2}tr \left[\begin{array}{c} \text{—}\boxed{U}\text{—}\boxed{e^{\alpha D}}\text{—}\boxed{U^\dagger}\text{—}\boxed{P_u}\text{—}\boxed{U}\text{—}\boxed{e^{\beta D}}\text{—}\boxed{U^\dagger}\text{—}\boxed{P_v}\text{—} \\ \text{—}\boxed{U}\text{—}\boxed{e^{\alpha D}}\text{—}\boxed{U^\dagger}\text{—}\boxed{P_u}\text{—}\boxed{U}\text{—}\boxed{e^{\beta D}}\text{—}\boxed{U^\dagger}\text{—}\boxed{P_v}\text{—} \end{array} \right]$$
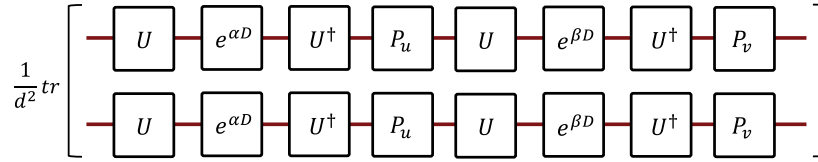
With simple manipulations, this can be redrawn as

$$\frac{1}{d^2}tr \left[\begin{array}{c} \text{—}\boxed{U}\text{—}\boxed{e^{\alpha D}}\text{—}\boxed{U^\dagger}\text{—}\boxed{P_u}\text{—}\searrow \\ \text{—}\boxed{U}\text{—}\boxed{e^{\beta D}}\text{—}\boxed{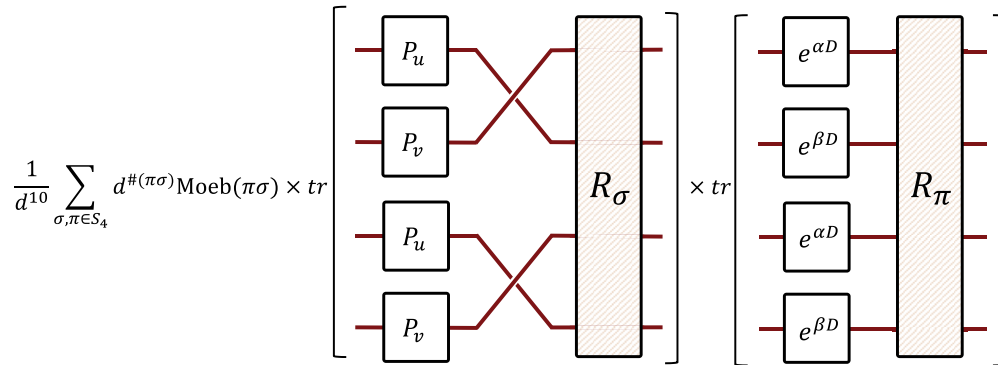U^\dagger}\text{—}\boxed{P_v}\text{—}\nearrow \\ \text{—}\boxed{U}\text{—}\boxed{e^{\alpha D}}\text{—}\boxed{U^\dagger}\text{—}\boxed{P_u}\text{—}\searrow \\ \text{—}\boxed{U}\text{—}\boxed{e^{\beta D}}\text{—}\boxed{U^\dagger}\text{—}\boxed{P_v}\text{—}\nearrow \end{array} \right]$$
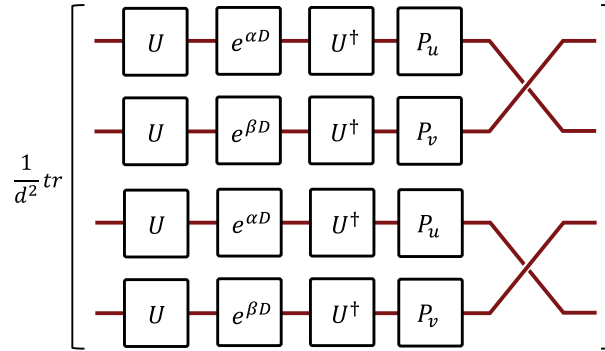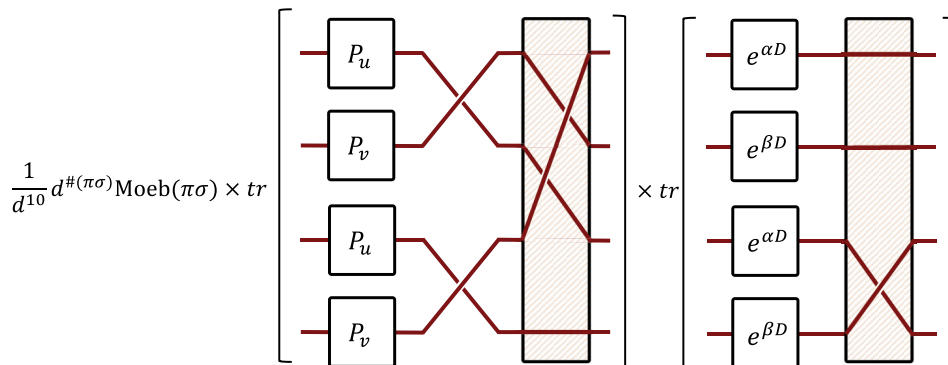
Define $\kappa := \left(\begin{smallmatrix} 1 & 2 & 3 & 4 \\ 2 & 1 & 4 & 3 \end{smallmatrix}\right)$ as the permutation that swaps the first and second Hilbert spaces and also the third and fourth (it has two swaps). Then, this shows that the quantity of interest is $\frac{1}{d^2} \text{tr}\left(U^{\otimes 4}\left[e^{\alpha D} \otimes e^{\beta D} \otimes e^{\alpha D} \otimes e^{\beta D}\right]U^{\dagger,\otimes 4}R_\kappa\right)$. Now, using Eq. (B9), we obtain the following formula for Eq. (C20):

$$\frac{1}{d^{10}}\sum_{\sigma,\pi \in S_4} d^{\#(\pi\sigma)}\text{Moeb}(\pi\sigma) \times tr\left[\begin{array}{c} \boxed{P_u} \\ \boxed{P_v} \\ \boxed{P_u} \\ \boxed{P_v} \end{array} \; R_\sigma \right] \times tr\left[\begin{array}{c} \boxed{e^{\alpha D}} \\ \boxed{e^{\beta D}} \\ \boxed{e^{\alpha D}} \\ \boxed{e^{\beta D}} \end{array} \; R_\pi \right]$$

There are $4! \times 4!$ terms in the sum but most of them are subleading in $d = 2^n$ [in fact, subleading in 2^{2n}, as the corrections to the Weingarten formulas are of order d^2 (see Ref. [53]) and can be neglected].

The calculation of each summand term is straightforward. For instance, if one uses $\sigma = \left(\begin{smallmatrix} 1 & 2 & 3 & 4 \\ 2 & 3 & 1 & 4 \end{smallmatrix}\right)$ and $\pi = \left(\begin{smallmatrix} 1 & 2 & 3 & 4 \\ 1 & 2 & 4 & 3 \end{smallmatrix}\right)$, then the corresponding term will be

$$\frac{1}{d^{10}}d^{\#(\pi\sigma)}\text{Moeb}(\pi\sigma) \times tr\left[\begin{array}{c} \boxed{P_u} \\ \boxed{P_v} \\ \boxed{P_u} \\ \boxed{P_v} \end{array} \right] \times tr\left[\begin{array}{c} \boxed{e^{\alpha D}} \\ \boxed{e^{\beta D}} \\ \boxed{e^{\alpha D}} \\ \boxed{e^{\beta D}} \end{array} \right]$$

which is equal to

$$\frac{1}{d^{10}} d^{\ell(\pi\sigma)} \text{Moeb}(\pi\sigma) \left(\text{tr}[P_{\mathbf{u}}P_{\mathbf{u}}P_{\mathbf{v}}] \text{tr}[P_{\mathbf{v}}]\right) \left(\text{tr}[e^{\alpha D}] \text{tr}[e^{\beta D}] \text{tr}[e^{(\alpha+\beta)D}]\right). \tag{C21}$$

This can be evaluated. One is able to read off the order of this term by replacing the tr with the normalized Tr:

$$\frac{1}{d^{10}} d^{\ell(\pi\sigma)} \text{Moeb}(\pi\sigma) \left(d^2 \text{Tr}[P_{\mathbf{u}}P_{\mathbf{u}}P_{\mathbf{v}}] \text{Tr}[P_{\mathbf{v}}]\right) \left(d^3 \text{Tr}[e^{\alpha D}] \text{Tr}[e^{\beta D}] \text{Tr}[e^{(\alpha+\beta)D}]\right). \tag{C22}$$

We define $\text{Tr}(e^{\alpha D}) = \text{Tr}(e^{\alpha H}) = f(\alpha)$, where $f(z)$ is the Fourier transform of the semicircle distribution,

$$f(z) = 2I_1(z)/z, \tag{C23}$$

and $I_1(z)$ is the modified Bessel function of the first kind of order 1. Note that each Tr is of $O(d^0)$, so the whole term is $O(d^{-5}d^{\ell(\pi\sigma)})$. We have $\pi\sigma = \left(\begin{smallmatrix} 1 & 2 & 3 & 4 \\ 2 & 3 & 4 & 1 \end{smallmatrix}\right)$, so $\ell(\pi\sigma) = 1$, the whole term is of order d^{-4}.

Similarly, for general π and σ, we have that the corresponding term is of the order of

$$d^{-10} d^{\ell(\pi\sigma)} \times d^{\ell(\kappa\sigma)} \times d^{\ell(\pi)} = d^{2-[\text{dist}(e,\pi)+\text{dist}(\pi,\sigma^{-1})+\text{dist}(\sigma^{-1},\kappa)]}. \tag{C24}$$

From the triangle inequality for the permutation-distance metric, we have that $\text{dist}(e,\pi) + \text{dist}(\pi,\sigma^{-1}) + \text{dist}(\sigma^{-1},\kappa) \geq \text{dist}(e,\kappa) = 2$. Hence, no term can be of positive order in d.

The complete calculation of $s(\alpha, \beta, \mathbf{u}, \mathbf{v})$ function to the leading order is tedious and can be computerized. We report the final result, to leading order in d, as calculated by computer:

$$s(\alpha, \beta, \mathbf{u}, \mathbf{v}) := \begin{cases} f(\alpha+\beta)^2, & \text{if } \mathbf{u} = \mathbf{v} = 0, \\ f(\alpha)^2 f(\beta)^2, & \text{if } \mathbf{u} = \mathbf{v} \neq 0, \\ \frac{1}{d^2}[f(2\alpha+2\beta) - f(\alpha+\beta)^2], & \text{if } \{\mathbf{u} = 0, \mathbf{v} \neq 0\} \text{ or } \{\mathbf{u} \neq 0, \mathbf{v} = 0\}, \\ \frac{1}{d^2}[f(2\alpha)f(\beta)^2 + f(2\beta)f(\alpha)^2 + f(\alpha+\beta)^2 - 3f(\alpha)^2 f(\beta)^2], & \text{if } \mathbf{u} \neq 0, \mathbf{v} \neq 0, \mathbf{u} \neq \mathbf{v}, [\mathbf{u}, \mathbf{v}] = 0, \\ \frac{1}{d^2}[f(\alpha)^2 f(\beta)^2 + f(\alpha+\beta)^2 - f(2\alpha)f(\beta)^2 - f(2\beta)f(\alpha)^2], & \text{if } \mathbf{u} \neq 0, \mathbf{v} \neq 0, \mathbf{u} \neq \mathbf{v}, [\mathbf{u}, \mathbf{v}] \neq 0. \end{cases} \tag{C25}$$

It is easy to read the *winding* size distribution of $\rho_\beta^{1/2} P_{\mathbf{u}}(t)$, defined in Eq. (2). If

$$\rho_\beta^{1/2} P_{\mathbf{u}}(t) = \frac{e^{(it-\beta/2)H} P_{\mathbf{u}} e^{-itH}}{\sqrt{df(-\beta)}} = \frac{1}{\sqrt{d}} \sum_{\mathbf{v}} c_{\mathbf{v}} P_{\mathbf{v}} \Rightarrow$$

$$\mathbb{E}(c_{\mathbf{v}})^2 = \frac{1}{d^2 f(-\beta)} \mathbb{E}\left(\text{tr}\left[e^{(it-\beta/2)H} P_{\mathbf{u}} e^{-itH} P_{\mathbf{v}}\right]\right)^2 = \frac{s(it-\beta/2, -it, \mathbf{u}, \mathbf{v})}{f(-\beta)}, \tag{C26}$$

this means that for large values of n, the winding size distribution is given by

$$q_{|\mathbf{u}|}(l) = \frac{\delta_{l,|\mathbf{u}|} f(it - \frac{\beta}{2})^2 f(-it)^2 + \text{N}(l; \mu = \frac{3n}{4}, \sigma = \sqrt{\frac{3n}{4}}) \left[f(-\frac{\beta}{2})^2 - f(it - \frac{\beta}{2})^2 f(-it)^2\right]}{f(-\beta)}. \tag{C27}$$

One can see that the function f is real on the real and imaginary line but becomes complex on the other parts of the complex plane. Therefore, the winding size distribution is real for $\beta = 0$ but it acquires a phase for nonzero values of t and β.

The calculations for the GOE are similar. The main differences are that one should use the elements of the Brauer algebra instead of permutations and use the Weingarten calculus for the orthogonal group. A complete and easy-to-read discussion of these techniques can be found in Ref. [53]. The eigenvalue distribution of the GOE is the same as for the GUE and follows the semicircle law [23].

3. 2-Local Brownian circuits

In this section, we focus on a different model of time evolution. Let us consider the model of fast scrambling studied in Ref. [26], a 2-local Brownian circuit. The main technical tool here is the Itô calculus.

We assume that the system is at infinite temperature and that the time evolution is given by a rapidly changing Hamiltonian. Suppose that at each instance of time, an operator evolves by the following rule:

$$O_t \to O_{t+dt} = e^{idH} O_t e^{-idH}. \tag{C28}$$

The infinitesimal time evolution dH is a 2-local Hamiltonian that has the following form:

$$dH = \frac{1}{\sqrt{8n}} \sum_{\mathbf{v}} dh_{\mathbf{v}} P_{\mathbf{v}}, \tag{C29}$$

where $\mathbf{v}$ is the vector indicating the Pauli term in the Hamiltonian. We assume that $dh_{\mathbf{v}}$ is only nonzero for terms that have 2 Paulis, for which it has mean 0 and $\mathbb{E}\, dh_{\mathbf{v}}^2 = dt$. We would like to read off the operator growth structure of such systems. First, we need to expand O_t in the Pauli basis:

$$O_t = \sum_{\mathbf{u}} c_{\mathbf{u}}(t) P_{\mathbf{u}}. \tag{C30}$$

As discussed before, $c_{\mathbf{u}}(t)$ averages to 0 and we are interested in $q_{\mathbf{u}}(t) = \mathbb{E}\, c_{\mathbf{u}}(t)^2$. To access $\mathbb{E} c_{\mathbf{u}}(t)^2$, look at $O_t \otimes O_t$:

$$O_t \otimes O_t = \sum_{\mathbf{uv}} c_{\mathbf{u}}(t) c_{\mathbf{v}}(t) P_{\mathbf{u}} \otimes P_{\mathbf{v}}. \tag{C31}$$

It is not hard to see that if $O_{t=0}$ is a single Pauli operator, then after averaging, only the diagonal term ($\mathbf{u} = \mathbf{v}$) survives in the above sum. Therefore, we obtain

$$\mathbb{E}\, O_t \otimes O_t = \sum_{\mathbf{u}} (\mathbb{E}\, c_{\mathbf{u}}(t)^2) P_{\mathbf{u}} \otimes P_{\mathbf{u}} = \sum_{\mathbf{u}} q_{\mathbf{u}}(t)\, P_{\mathbf{u}} \otimes P_{\mathbf{u}}. \tag{C32}$$

Now, we have

$$\mathbb{E}\, O_{t+dt} \otimes O_{t+dt} = \mathbb{E}\Big(\big[e^{idH} \otimes e^{idH}\big] (O_t \otimes O_t) \big[e^{-idH} \otimes e^{-idH}\big] \Big) = \sum_{\mathbf{u}} q_{\mathbf{u}}(t)\, \mathbb{E}\Big(\big[e^{idH} \otimes e^{idH}\big] P_{\mathbf{u}} \otimes P_{\mathbf{u}} \big[e^{-idH} \otimes e^{-idH}\big] \Big). \tag{C33}$$

Using the rules of Itô calculus,

$$\mathbb{E}\Big(\big[e^{idH} \otimes e^{idH}\big] P_{\mathbf{u}} \otimes P_{\mathbf{u}} \big[e^{-idH} \otimes e^{-idH}\big] \Big)$$

$$= P_{\mathbf{u}} \otimes P_{\mathbf{u}} + \mathbb{E}\Big([dH \otimes I + I \otimes dH] P_{\mathbf{u}} \otimes P_{\mathbf{u}} [dH \otimes I + I \otimes dH] - \frac{1}{2}\big\{ [dH \otimes I + I \otimes dH]^2, P_{\mathbf{u}} \otimes P_{\mathbf{u}} \big\} \Big)$$

$$= P_{\mathbf{u}} \otimes P_{\mathbf{u}} + \frac{\mathbb{E}\,(dh_{\mathbf{v}}^2)}{8n} \sum_{\mathbf{v}} \Big([P_{\mathbf{v}} \otimes I + I \otimes P_{\mathbf{v}}] P_{\mathbf{u}} \otimes P_{\mathbf{u}} [P_{\mathbf{v}} \otimes I + I \otimes P_{\mathbf{v}}] - \frac{1}{2}\big\{ [P_{\mathbf{v}} \otimes I + I \otimes P_{\mathbf{v}}]^2, P_{\mathbf{u}} \otimes P_{\mathbf{u}} \big\} \Big)$$

$$= P_{\mathbf{u}} \otimes P_{\mathbf{u}} + \frac{dt}{2n} \sum_{\mathbf{v}, P_{\mathbf{v}} \text{ is a 2-Pauli operator}} (P_{\mathbf{v+u}} \otimes P_{\mathbf{v+u}} - P_{\mathbf{u}} \otimes P_{\mathbf{u}}) \times \delta(P_{\mathbf{u}} \& P_{\mathbf{v}} \text{ anticommute}), \tag{C34}$$

where we use the notation that $\delta(P_{\mathbf{u}} \& P_{\mathbf{v}} \text{ anticommute})$ is equal to one if $P_{\mathbf{u}}$ and $P_{\mathbf{v}}$ anticommute and zero otherwise. Hence, we obtain the following formula by change of variables in the first sum:

$$\frac{d}{dt} \mathbb{E}\,(O_t \otimes O_t) = \frac{1}{2n} \sum_{\mathbf{u}} \sum_{\mathbf{v}, P_{\mathbf{v}} \text{ is a 2-Pauli operator}} P_{\mathbf{u}} \otimes P_{\mathbf{u}} \times [q_{\mathbf{u+v}}(t) - q_{\mathbf{u}}(t)] \times \delta(P_{\mathbf{u}} \& P_{\mathbf{v}} \text{ anticommute}). \tag{C35}$$

This gives the following simple update rule for $q_{\mathbf{u}}(t)$:

$$\frac{d}{dt}q_{\mathbf{u}}(t) = \frac{1}{2n} \sum_{\mathbf{v},P_{\mathbf{v}} \text{ is a 2-Pauli operator}} [q_{\mathbf{u+v}}(t) - q_{\mathbf{u}}(t)] \times \delta(P_{\mathbf{u}}\&P_{\mathbf{v}} \text{ anticommute}). \tag{C36}$$

Let's define, as before, the winding size distribution on operators of certain size by $q_l(t) = \sum_{|\mathbf{u}|=l} q_{\mathbf{u}}(t)$. Using some combinatoric equalities, one arrives at $q_l(t)$:

$$\frac{d}{dt}q_l(t) = n\left[3\left(\frac{l}{n} - \frac{1}{n}\right)\left(1 - \frac{l}{n} + \frac{1}{n}\right)q_{l-1}(t) + \frac{l}{n}\left(\frac{l}{n} + \frac{1}{n}\right)q_{l+1}(t) - \left[3\frac{l}{n}\left(1 - \frac{l}{n}\right) + \frac{l}{n}\left(\frac{l}{n} - \frac{1}{n}\right)\right]q_l(t)\right]. \tag{C37}$$

If we define $\Phi(x, t) = q_{nx}(t)$ and $\Delta x = 1/n$, we have for $x = k\Delta x, (k \in \mathbb{N})$,

$$\frac{d}{dt}\Phi(x, t) = \left[3(x - \Delta x)(1 - x + \Delta x)\Phi(x - \Delta x, t) + x(x + \Delta x)\Phi(x + \Delta x, t) - \left[3x(1 - x) + x(x - \Delta x)\right]\Phi(x, t)\right] / \Delta x \tag{C38}$$
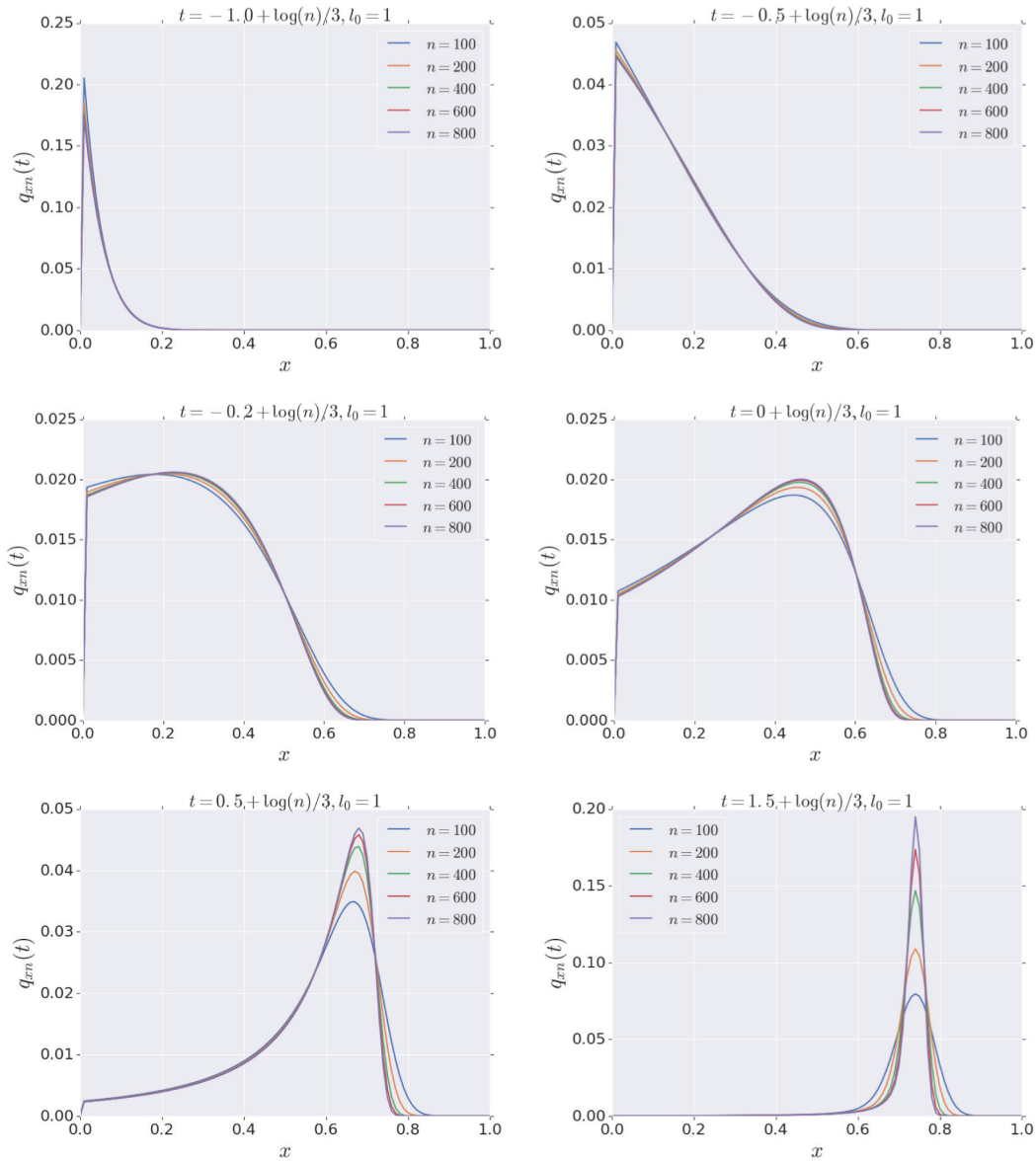
(for solutions, see Figs. 14 and 9).

FIG. 14. The Brownian-circuit operator growth as function of the number of qubits and the initial time.

From Fig. 14, one can see that the operator size distribution Φ is to a great extent independent of n and follows the same form as long as one modifies t by adding a logarithmic term in n into t. In other words, the function $\hat{\Phi}(x, t) = \Phi(x, t + \log(n)/3)$ seems to be n independent in the large-n limit and at times slightly smaller than the scrambling time. It is important to point out that for very late times, the distribution becomes Gaussian, with a standard deviation proportional to $\sqrt{n}$; hence the diagrams are much sharper for larger n and late times.

4. Size winding in the SYK model from Qi-Streicher formalism

In this section, we use the machinery developed by Qi and Streicher [11] to study the SYK model in the large-q limit. We demonstrate that in that in some limit (to be specified later), size winding happens in a perfectly linear and *detailed* way.

In Ref. [11], the authors study the size operator defined with the conventional absolute-value notation (see Ref. [Sec. 3.1] [11]). Now, we contrast their definition and what we define as the winding size distribution. Let $\rho_\beta^{1/2} \Psi_1(t) = \sum_u c_u \Psi_u$, where Ψ_1 is a single fermion operator and the sum is over the index set $u \in \{0, 1\}^n$, with each u_i indicating whether the compound fermionic operator Ψ_u has a fermion on site i. For the convenience of the reader, we used definitions from earlier sections of the manuscript. The conventional size distribution of the operators is implicitly defined in Ref. [11] by

$$\mathcal{P}_l\left[\rho_\beta^{1/2} \Psi(t)\right] = \sum_{|u|=l} |c_u|^2. \tag{C39}$$

The *winding* size distribution is defined without the absolute value:

$$q_l\left[\rho_\beta^{1/2} \Psi(t)\right] = \sum_{|u|=l} c_u^2. \tag{C40}$$

Size winding, in its perfect form, is the following ansatz for the operator wave function:

$$c_P = e^{i\alpha|P|/n} r_P. \quad r_P \in \mathbb{R}. \tag{C41}$$

Our goal in this appendix is to check from an SYK calculation that size winding holds by verifying that

$$q(\ell) = \mathcal{P}(\ell) e^{i\gamma \ell} \tag{C42}$$

for some γ. Qi and Streicher define the *growth distribution* $K_n^\beta[\Psi(t)]$ such that the size distribution of $P_n[\Psi(t)\rho_\beta^{1/2}]$ is given as the convolution of the size distribution of $\rho_\beta^{1/2}$ and

the growth distribution:

$$\mathcal{P}_n\left[\rho_\beta^{1/2} \Psi(t)\right] = \sum_m \mathcal{P}_{n-m}\left[\rho_\beta^{1/2}\right] K_m^\beta[\Psi(t)]. \tag{C43}$$

For teleportation purposes, we are interested in the winding size distribution $q(l)$ defined in Eq. (2). Indeed, as ρ_β is Hermitian, there is no difference between $q(l)$ and P_m for the thermal state. By explicitly computing the two-point function, the authors of Ref. [11] have derived the form of the growth distribution.

The distribution of K_l^β in Ref. [11] can be written as a negative binomial distribution, NB, which is a distribution with two parameters r and p, defined as

$$\mathrm{NB}(l; r, p) := (1 - p)^r \binom{l + r - 1}{l} p^l. \tag{C44}$$

This distribution is generically useful for fitting overdispersed data, as a NB can have a standard deviation that as large as its mean. The mean and variance of a NB are given by

$$\text{mean: } \frac{pr}{1 - p}, \qquad \text{standard deviation: } \frac{\sqrt{pr}}{1 - p}. \tag{C45}$$

For the case of the SYK model [11], we show that

$$K_{l=\delta_\beta(1+qm)}^\beta = \mathrm{NB}\left(m; 2/q, \frac{\left[\frac{J}{\alpha} \sinh(\alpha t)\right]^2}{1 + \left[\frac{J}{\alpha} \sinh(\alpha t)\right]^2}\right), \tag{C46}$$

where α is the first positive root of

$$\alpha = J \sin(\gamma), \quad \text{and } \sin(\alpha\beta/2 + 2\gamma) = \sin(\alpha\beta/2), \tag{C47}$$

and

$$\delta_\beta = \left(\frac{\alpha}{J}\right)^{2/q}. \tag{C48}$$

For very large β (small temperature), these can be expanded as

$$\alpha = \frac{\pi}{\beta} - \frac{2\pi}{\beta^2 J} + O(1/\beta^3), \quad \gamma = \frac{\pi}{\beta J} - \frac{2\pi}{\beta^2 J^2} + O(1/\beta^3) \tag{C49}$$

and the average of the growth distribution, K_l^β, is

$$\begin{aligned}\Delta n &= \delta_\beta\left(1 + q\frac{2/q}{1 - \frac{\sinh(\alpha t)^2}{1 + \sinh(\alpha t)^2}}\right) \\ &= \delta_\beta\left(1 + 2\left[\frac{J}{\alpha} \sinh(\alpha t)\right]^2\right),\end{aligned} \tag{C50}$$

with the standard deviation $\sigma(n) \approx \sqrt{q/(2)} \Delta n$.

In the SYK model, the width of the size distribution of the thermal state is small, of order $\sqrt{n}$. We are interested in studying the system at times slightly before the scrambling time, when the formalism of Ref. [11] is valid and the width of the size distribution of $\Psi(t)\rho_\beta^{1/2}$ is a small fraction of n. In this regime, we have $1 \ll \sinh(\alpha t) \approx e^{\alpha t}$ and we obtain

$$K_{l=\delta_\beta(1+qm)}^\beta = \mathrm{NB}\left(m; 2/q, \frac{1}{1+4\frac{\alpha^2}{J^2}e^{-2\alpha t}}\right) \quad (C51)$$

$$\approx \left(4\frac{\alpha^2}{J^2}e^{-2\alpha t}\right)^{2/q} \times \binom{m+2/q-1}{m}$$

$$\times \left[1 - 4\frac{\alpha^2}{J^2}e^{-2\alpha t}\right]^m. \quad (C52)$$

In this limit, it is clear that K_l^β dictates the size distribution P_m, as the thermal state acts as a delta function in the convolution formula given in Eq. (C43).

Now, we would like to find the growth distribution for the winding size distribution q_l, which we call the *winding growth distribution* $\tilde{q}_l^\beta$. We can see that similar to K_l^β, $\tilde{q}_l^\beta$ dictates the q_l distribution at the time regime of interest (slightly before the scrambling rime). To compute the winding size distribution, one can analytically continue Eq. (4.9) of Ref. [11] and set $\tau_1 = \beta/4 - it$, $\tau_2 = -\beta/4 - it$ to derive a formula for $\tilde{q}_l^\beta$, which, with minor simplifications, leads to

$$\sum_{l=0}^m \tilde{q}_l^\beta e^{-\mu l} = \frac{e^{-\mu\delta_\beta}G}{\left[1-(1-e^{-\mu\delta_\beta q})\frac{\sin(it\alpha_\mu)\sin(\alpha_\mu\beta/2+it\alpha_\mu)}{\sin(\gamma_\mu)\sin(\alpha_\mu\beta/2+\gamma_\mu)}\right]^{2/q}}. \quad (C53)$$

Here, we define $G := \left[\sin(\gamma_\mu)/\sin(\alpha_\mu\beta/2+\gamma_\mu)\right]^{2/q}$; α_μ and γ_μ are functions of μ through the analog of Eq. (C47),

$$\alpha_\mu = J\sin(\gamma_\mu), \quad \text{and} \quad \sin(\alpha_\mu\beta/2+2\gamma_\mu)$$

$$= e^{-\mu\delta_\beta q}\sin(\alpha_\mu\beta/2), \quad (C54)$$

and α_μ is the smallest positive root of the above equation.

One can simply expand Eq. (C53) in terms of binomial coefficients to obtain the following relation for the winding growth distribution:

$$\sum_{l=0}^m \tilde{q}_l^\beta e^{-\mu l} = \frac{G}{[1-h_\mu(t)]^{2/q}} \sum_{m=0}^\infty \binom{-2/q}{m}\left(\frac{h_\mu(t)}{1-h_\mu(t)}\right)^m$$

$$\times e^{-\mu\delta_\beta(1+qm)}, \quad (C55)$$

where

$$h_\mu(t) := \frac{\sin(it\alpha_\mu)\sin(\alpha_\mu\beta/2+it\alpha_\mu)}{\sin(\gamma_\mu)\sin(\alpha_\mu\beta/2+\gamma_\mu)}. \quad (C56)$$

We are interested at times where $\tilde{q}_l^\beta$ is a very wide distribution, with a width of $O(n)$. To read such low-frequency structure from $\sum_{l=0}^m \tilde{q}_l^\beta e^{-\mu l}$, we have to look at μ of $O(1/n)$. In that regime, $G = \delta_\beta$, and α_μ and γ_μ are frozen to be very close their value for $\mu = 0$ and given by Eq. (C47). With this approximation, we establish that

$$\tilde{q}_{l=\delta_\beta(1+qm)}^\beta = \frac{\delta_\beta}{[1-h_0(t)]^{2/q}} \times \binom{m+2/q-1}{m}$$

$$\times \left(\frac{h_0(t)}{h_0(t)-1}\right)^m$$

$$= \delta_\beta\,\mathrm{NB}\left(m; 2/q, \frac{h_0(t)}{h_0(t)-1}\right). \quad (C57)$$

From this equation, it is clear that there should exist a linear phase in $\hat{q}(l)$: it is the phase of $(h_0(t))/(h_0(t)-1)$ that accumulates as l increases. We can compute $h_0(t)$ for very small temperatures using the expansion in Eq. (C49):

$$h_0(t) = \frac{\sin(it\alpha_\mu)\sin(\alpha_\mu\beta/2+it\alpha_\mu)}{\sin(\gamma_\mu)\sin(\alpha_\mu\beta/2+\gamma_\mu)}$$

$$\approx i\sinh(\alpha t)\left(\frac{\beta J}{\pi}\cosh(\alpha t) + i\sinh(\alpha t).\right) \quad (C58)$$

We have already concluded that in the time regime of interest, $\sinh(\alpha t) \approx \cosh(\alpha t) \approx e^{\alpha t}/2$ and, therefore,

$$h_0(t) \approx \frac{e^{2\alpha t}}{4}\left(i\frac{J}{\alpha}-1\right). \quad (C59)$$

Now, we can compute the quantity $(h_0(t))/(h_0(t)-1)$:

$$\frac{1}{1-1/h_0(t)} \approx e^{1/h_0(t)}$$

$$= \left[1-4\frac{\alpha^2}{J^2}e^{-2\alpha t}\right]\exp\left(-i4\frac{\alpha}{J}e^{-2\alpha t}\right). \quad (C60)$$

Let us compare the absolute value of the winding growth distribution $\left|\tilde{q}_l^\beta\right|$ with the ordinary growth distribution K_l^β. At the times of interest,

$$\frac{\delta_\beta}{|1-h_0(t)|^{2/q}} \approx \frac{\delta_\beta}{\left(\frac{J}{\alpha}\frac{e^{2\alpha t}}{4}\right)^{2/q}} = \left(4\frac{\alpha^2}{J^2}e^{-2\alpha t}\right)^{2/q}, \quad \text{and,} \quad (C61)$$

$$\left|\frac{h_0(t)}{1-h_0(t)}\right| \approx \left[1-4\left(\frac{\alpha}{J}\right)^2 e^{-2\alpha t}\right]. \quad (C62)$$

Comparing this and Eq. (C51), one can verify that the distributions of $\left|\tilde{q}_l^\beta\right|$ and K_l^β are identical. This indicates that

the winding size distribution is indeed the ordinary size distribution with a linearly growing phase.

The wavelength of the size winding can be read from Eq. (C60). The size distribution winds by $4\frac{\alpha}{J}e^{-2\alpha t}$ for each $\delta_\beta q$ increase in size. This gives the following wavelength for the size winding λ_S:

$$
\lambda_s = \delta_\beta \frac{\pi}{2} \frac{J}{\alpha} q e^{2\alpha t} \approx \pi q \frac{\alpha}{J} \Delta n \approx \frac{\pi^2 q}{\beta J} \Delta n \implies \Delta n/\lambda_s
$$
$$
\approx \frac{\beta J}{\pi^2 q}. \qquad (C63)
$$

Hence, the winding size distribution has $\beta J/(\pi^2 q)$ windings per standard deviation of the size distribution. This can become large as one decreases the temperature. We point out that the initial phase of the size distribution, i.e., the phase of $\tilde{q}^{\beta}_{(l=0)}$, is equal to $-\pi/q$.

We note that size winding without significant damping of the absolute value implies a strong form of winding, which we call *detailed* winding. For simplicity, let us go back to the qubit picture and assume size winding without damping. Because $q_l = e^{i\theta}K_l$, we have that

$$
\sum_{|P|=l} c_P^2 = e^{i\theta} \sum_{|P|=l} |c_P|^2. \qquad (C64)
$$

This shows that for all P with $|P| = l$, $c_P = \pm e^{i\theta/2}|c_P|$. One can reasonably argue that all c_P's have the same sign—say, the plus sign—and therefore we have $c_P = e^{i\theta/2}|c_P|$. This shows not only that the size distribution winds in a linear way but that all of the individual Pauli (or fermion) coefficients collectively wind by phase proportional to their size. This is a quite strong condition, which we believe is a strong sign of having a holographic dual. Indeed, if one considers the low-temperature GUE, then the size winding happens, but as the size winds, the absolute value of the winding size damps, an indication that detailed winding is missing in that model.

APPENDIX D: STRINGY EFFECTS IN THE LARGE-*q* SYK MODEL

Here, we analyze the traversable wormhole at finite βJ and infinite $q^2 \ll N$ (and finite instantaneous coupling between the two sides). In this appendix, we use N as the total number of Majorana fermions in order to be consistent with the quantum gravity literature. We also first discuss the case where g/N is small. This section starts in parallel with Appendix C 4 but the approximations and techniques will diverge. In particular, we will compare the SYK results with expectations from string theory. For the convenience of the reader, we restate the Qi-Streicher calculations. We take their twisted two-point function and

analytically continue:

$$
\begin{aligned}
\tau_1 &= \beta/4 + it_r, \\
\tau_2 &= -\beta/4 - it_l, \qquad (D1) \\
\hat{\mu} &= -ig/N.
\end{aligned}
$$

For simplicity, let us set $t_l = -t_r = t$. Using their twisted two-point function, we obtain

$$
\mathcal{G} = \frac{e^{ig/N}G(\beta/2)}{[1 - z\sinh(\alpha t)\sinh(\alpha t - i\alpha\beta/2)]^{2/q}},
$$
$$
z = -\mathcal{J}\left(\frac{1 - e^{ig/N}}{\alpha}\right) \approx \frac{ig\mathcal{J}}{N\alpha}. \qquad (D2)
$$

The approximation in the last line is that g/N is small. The two-point function $G(\beta/2)^{q/2} = \alpha/\mathcal{J}$. This equation is derived by finding a classical solution of the large-q effective action, which has the form of a Liouville action. The boundary conditions determine α in terms of the parameters (g/N) and $\beta\mathcal{J}$. Note that when the real part of $\alpha t \gg 1$, we can replace the factor in the denominator:

$$
G \approx e^{ig/N}\frac{G(\beta/2)}{[1 - \tilde{z}e^{2\alpha t}]^{2/q}},
$$
$$
\tilde{z} = \frac{z}{4}e^{-i\alpha\beta/2} = -i\frac{z}{4}e^{i\pi(1-v)/2} \approx \frac{g\mathcal{J}}{4N\alpha}e^{i\pi(1-v)/2}. \qquad (D3)
$$

For small g, $\tilde{z}$ is a complex number that is proportional to g. The phase of $\tilde{z}$ is important. Note that the phase is nonzero. Let us write it once more in the small-g/N approximation and using the Maldacena-Stanford [57] notation $\alpha = \pi v/\beta$, where v is the fraction of the maximum Lyapunov exponent $\lambda = 2\pi v/\beta$:

$$
G \approx \left[\frac{\pi v/(\beta\mathcal{J})}{1 - g\frac{\beta\mathcal{J}}{4N\pi v}e^{i\pi(1-v)/2}e^{2\pi vt/\beta}}\right]^{2/q}. \qquad (D4)
$$

Here, we see that g should be positive. This formula is supposed to be valid in a limit where $g/N \to 0$ but $ge^{2\alpha t}/N$ is held finite.

Note that at very low temperatures, $v = 1$, so we expect the Schwarzian computations with probe particles of Ref. [6] to be valid. More explicitly, if we set $t_l = -t_r = t$, then $G(t) \sim (1 - \#gG_Ne^t)^{-2/q}$, which is indeed their probe-particle formula.

One feature of this formula is that there is a pole at some t (roughly the scrambling time). In the probe limit, this is supposed to be smoothed out by stringy effects. Here, we see indeed that finite-temperature effects can smooth out the pole; in particular, when for finite temperature, $0 < v < 1$ and we see that the nontrivial phase in the prefactor shifts the pole away from the real t axis. Note also

that for finite v, we get an imaginary part to this correlation function immediately. Therefore, the discussion is very similar to that of Maldacena *et al.* [6], where stringy effects give rise to a (small) immediate signal between the two sides.

One interesting aspect about this formula is that it looks very much as though we are acting with some nonunitary deformation of the symmetry generator P_+:

$$C = \left\langle \phi_L e^{-ia^+(1-i\epsilon)P_+} \phi_R \right\rangle. \qquad (D5)$$

This looks morally like the stringy effects discussed in Ref. [6] but it seems simpler than what we would have naively expected. In particular, it seems that there is no distortion.

To complete this discussion, we should solve for α or, equivalently, for v. The boundary conditions to the Liouville equation give

$$\alpha = \mathcal{J} \sin\gamma, \quad \sin(\alpha\beta/2 + 2\gamma) = e^{ig/N} \sin\left(\frac{\alpha\beta}{2}\right). \qquad (D6)$$

To leading order in small g/N, we can in fact ignore g and just use the solution discussed in Maldacena-Stanford [57]. This solution has the asymptotics

$$\alpha = \frac{\pi v}{\beta}, \quad v = 1 - \frac{2}{\beta\mathcal{J}} + \mathcal{O}\left(\frac{1}{\beta\mathcal{J}}\right)^2,$$

$$v = \frac{\beta\mathcal{J}}{\pi} - \frac{(\beta\mathcal{J})^3}{8\pi}. \qquad (D7)$$

If we go to very high temperatures, $v \to 0$ and the phase becomes purely imaginary. Expanding the denominator in Eq. (D11), we obtain

$$\text{Im } C \approx \frac{2g}{qN} \sinh^2(\mathcal{J}t). \qquad (D8)$$

An important point is that we have no reason to trust these calculations at or beyond the scrambling time, when back reaction is important. To be a little bit more precise, we can consider the probe limit in gravity. Since a fermion adds a finite amount of energy of order approximately $\mathcal{J}$, we should smear the wave functions slightly. The analysis of Ref. [6] shows that the probe limit is only good in the regime $\Delta\hat{g}G_N e^t \ll \hat{g}^{1/2+q/4}$.

1. UV regulator

Here, we would like to compare the twisted two-point function in the large-q model to the one predicted by the Schwarzian. This allows us to fix the UV regulator, which

can be thought of as the leading correction in $1/\beta\mathcal{J}$ to the Schwarzian answer. First, recall that the Schwarzian gives

$$\mathcal{C}_{\text{Sch}}(t_L, t_R) \propto \frac{1}{\left(4\cosh\frac{t_L+t_R}{2} - \tilde{g}e^{\frac{t_R-t_L}{2}}\right)^{2\Delta}}. \qquad (D9)$$

Specializing to $t_L = -t_R = t + i\epsilon$ and restoring units, we obtain

$$\mathcal{C}_{\text{Sch}} \propto \left(1 - \frac{\tilde{g}}{4}e^{2\pi t/\beta + 2\pi i\epsilon/\beta}\right)^{-2\Delta}, \quad \tilde{g} = g\beta\mathcal{J}/(\pi N). \qquad (D10)$$

On the other hand, the finite-temperature large-q answer in the appropriate limit gives

$$\mathcal{C} \propto \left[1 - \frac{\tilde{g}}{4v}e^{i\pi(1-v)/2}e^{2\pi vt/\beta}\right]^{-2/q}. \qquad (D11)$$

At low temperatures, the phase gives $1 - v = 2/\beta\mathcal{J}$. This can be absorbed into the above formulas by setting $\epsilon = 1/2\mathcal{J}$.

On the other hand, to compute $\mathcal{P}(s, t)$ we set $t_L = -t + i\pi + i\epsilon'$, $t_R = t + i\epsilon'$:

$$\mathcal{C}_{\mathcal{P}} \propto \left(\frac{4\pi\epsilon'}{\beta} - \frac{i\tilde{g}}{2}e^{2\pi t/\beta}\right)^{-2\Delta} \propto \left(1 - \frac{i\tilde{g}\beta}{8\pi\epsilon'}e^{2\pi t/\beta}\right)^{-2\Delta}. \qquad (D12)$$

Comparing with Eq. (5.5) in Qi and Streicher [11],

$$\mathcal{G}_\mu\left(\frac{\beta^+}{4} + it, \frac{\beta^-}{4} + it\right) \approx \left(1 - \frac{z\mathcal{J}}{4\alpha}e^{2\alpha t}\right)^{-2/q}$$

$$\approx \left(1 - \frac{i\tilde{g}}{4\pi v^2}\beta\mathcal{J}e^{2\pi t/\beta}\right)^{-2/q}. \qquad (D13)$$

In the low-temperature limit, $v \to 1$, so

$$\epsilon' = \frac{1}{2\mathcal{J}} = \epsilon. \qquad (D14)$$

However, note that even at finite temperature, both correlators have the same form if we simply rescale $\beta \to \beta/v$.

2. Higher order in g/N effects

We can, in principle, extend the above discussion to higher order in g/N. This is a scaling limit, where $N \to \infty$ and $g \to \infty$, with g/N fixed but small, so we only sum $1/N$ effects that are multiplied by the appropriate powers of g.

Let us first work out the perturbative in g/N corrections to α. We can go to very low temperatures first, where $v = 1$. We would now like to solve this for nontrivial g. Expanding perturbatively around the $g = 0$ solution,

$$\alpha \approx \gamma, \quad \left[2 - \left(\frac{\alpha\beta}{2} + 2\gamma - \frac{\pi}{2} \right)^2 \right]$$

$$\approx e^{-\mu} \left[2 - \left(\frac{\alpha\beta}{2} - \frac{\pi}{2} \right)^2 \right], \tag{D15}$$

so the leading-order correction to α is

$$\alpha = \frac{\pi}{\beta} - i \frac{g}{\pi N}, \quad G(\beta/2)^{q/2} = \alpha/\mathcal{J}, \tag{D16}$$

$$G = \frac{G(\beta/2)}{\left[1 - \frac{g\beta\mathcal{J}}{\pi N} e^{2\alpha t} \right]^{2/q}}. \tag{D17}$$

We have already discussed how finite-temperature effects remove the divergence for real values of t. Here, it seems that finite-g/N effects can do the same; at the very least, a complex value of α will shift the pole. Therefore, both $\tilde{z}$ and α will be complex and can smooth out the pole.

One question is as follows: what is the maximum imaginary value of this correlator? The maximum value is interesting because it is one way of quantifying how well the signal gets transmitted. This seems to be sensitive to the imaginary contribution to α. Note that if we stay within this approximation, this question is somewhat artificial, because back reaction could presumably change the answer a lot.

For a more general value of $\beta\mathcal{J}$ and g, we could numerically solve for α using Eq. (D6). In general, it seems that there will be many solutions to Eq. (D6). We should find the solution with minimum action. For small g/N, we can probably ignore this by first finding the solution at $g = 0$ (the usual chaos exponent) and then using this as a starting point for a numerical search.

3. Comparison with gravity

Here, we review the stringy traversable wormhole calculation of Maldacena *et al.* [6,58]. We start by considering the gravitational scattering of a particle with wave function ψ against n particles, each in state χ,

$$\langle \phi_L (O_L O_R)^n \phi_R \rangle$$

$$= \int dp_+ \psi_L^*(p_+) \psi_R(p_+) \left[\int dq_- e^{iS} \chi_L^*(q_-) \chi_R(q_-) \right]^n. \tag{D18}$$

Here, we have in mind a picture where the χ particles start out on the left side and propagate to the right and the ψ particles start on the right and propagate to the left side. Then summing over n gives us the correlator

$$\tilde{C} \equiv \langle \phi_L e^{igV} \phi_R \rangle = \int dp \; \psi_L^*(p) \psi_R(p)$$

$$\times \exp \left[ig \int dq_- e^{iS} \chi_R^*(q_-) \chi_L(q_-) \right]. \tag{D19}$$

In the probe limit, we assume that the shock-wave action S is small, so that the amplitude is approximately $e^{iS} \approx 1 + iS$.

If we are interested in a very-low-temperature setup, we can ignore all stringy effects. Then, the gravitational shock-wave amplitude is determined by the on-shell action $S = G_N e^t p_+ q_-$. Furthermore, the momentum wave functions are determined by conformal symmetry:

$$\psi_L^*(p_+) \psi_R(p_+) = \frac{1}{\Gamma(2\Delta)} \frac{1}{(-p_+)} (2ip_+)^{2\Delta} e^{-4ip_+} \Theta(-p_+), \tag{D20}$$

and similarly for the momentum wave functions q_-. This allows us to easily compute the average momentum of the shock wave, which is just a number that depends on Δ.

This allows us to simplify the exponent

$$igV \approx \frac{ig}{2^{2\Delta+1}} \left(p_+ G_N e^t \Delta + 2 \right). \tag{D21}$$

We we arrive at the *probe-particle formula:*

$$C_{\text{probe}} = e^{-i\frac{g}{2^{2\Delta}}} \tilde{C} = \int dp_+ \psi_L(p_+)^* \psi_R(p_+) e^{-ia^+ p_+}$$

$$= \langle \phi_L e^{-ia^+ \hat{P}_+} \phi_R \rangle = \frac{1}{(2 + \frac{a^+}{2})^{2\Delta}},$$

$$a^+ = -\Delta \frac{g}{2^{2\Delta+1}} G_N e^t. \tag{D22}$$

Now, in string theory, the shock-wave amplitude gets modified:

$$iS = -G_N \left(-ie^t p_+ q_- \right)^v = iG_N e^{i\pi(1-v)/2} \left(p_+ q_- e^t \right)^v. \tag{D23}$$

Here, $0 < v < 1$ and is related to the stringy-chaos exponent. In the probe limit,

$$C_{\text{probe}}^{\text{stringy}} = \int dp_+ \psi^*(p_+) \psi(p_+)$$

$$\times \exp \left[-igG_N \int dq_- (-ip_+ q_- e^t)^v \right.$$

$$\left. \times \psi^*(q_-) \psi(q_-) \right]. \tag{D24}$$

Now note that when stringy effects are important, e.g., in the SYK model at finite temperature, the wave functions can also change, since at finite temperature they are no longer determined by conformal symmetry. In general, we do not know how to determine $\psi_v(p_+)$ but in the large-q limit, we have a specific proposal:

$$dp_+\psi_{L,v}^*(p_+)\psi_{R,v}(p_+) = dp_+^v\psi_{L,1}^*(p_+^v)\psi_{R,1}(p_+^v). \quad \text{(D25)}$$

Therefore, defining $\mathfrak{p}_+ = p_+^v$, we have

$$C_{\text{probe}}^{\text{stringy}} = \int d\mathfrak{p}_+ \psi^*(\mathfrak{p}_+)\psi(\mathfrak{p}_+) \exp\left[-igG_N \int d\mathfrak{q}_- \, \mathfrak{p}_+ \right.$$

$$\left. \times \, \mathfrak{q}_- e^{v(t-i\pi/2)}\psi^*(\mathfrak{q}_-)\psi(\mathfrak{q}_-)\right]. \quad \text{(D26)}$$

This gives the simple answer

$$C = \left[2 + \frac{a^+ e^{i\pi(1-v)/2}}{2}\right]^{-2\Delta}, \quad a^+ \propto -gG_N e^{vt}, \quad \text{(D27)}$$

which agrees precisely with the large-q calculation.

Note that we derive the analog of the stringy-probe formula. However, once we determine the S matrix and the wave functions, we can use the string ansatz to go beyond the probe approximation. In other words, the ansatz we have written down gives some predictions for $1/N$ corrections to the 4-point function. It would be nice to check these against SYK results.

Some of the formulas in this section have also been derived in Ref. [59]. The main novelty here is that a simple change in the wave functions allows for a quantitative match with stringy formulas.

APPENDIX E: ENTANGLEMENT ENTROPY IN NEARLY AdS₂ GRAVITY

Here, we compute some entanglement entropies in the global vacuum state of AdS_2. Global AdS_2 is topologically a strip. In general, we should specify boundary conditions for the strip. We consider standard "reflecting" boundary conditions. We can use a "doubling" trick to relate this state to the state on a topological cylinder. (This is similar to a trick familiar from studying the world sheet of string theory, which relates the open string to the closed string.) We can imagine joining such that the left-moving modes live on one side of the strip and the right-moving modes move on the other side. Then, at each boundary, we join the left movers to the right movers. If the quantum fields are conformal, we have a simple expression for the entanglement entropy of a single interval $[\theta_1, \theta_2]$ on a cylinder:

$$S \sim \frac{c}{6} \log\left[\frac{\sin^2(\theta_1 - \theta_2)/2}{\epsilon_1\Omega_1\epsilon_2\Omega_2}\right]. \quad \text{(E1)}$$

Here, Ω is the warp factor and ϵ is some small UV regulator, which we ignore (in the generalized entropy, it contributes to the renormalization of S_0). Now, for AdS_2 in global coordinates, $\Omega = \sin\sigma$. Note that if we compute the entropy of an interval that includes the asymptotic left side of AdS_2 (at $\sigma = 0$) and ends at some other value σ, we should set $\theta_1 = -\theta_2 = \sigma$. Then, we find that the entropy of that interval is independent of the endpoint σ, as required by the AdS_2 isometries. However, the entropy of a single interval with endpoints σ_1 and σ_2 in AdS_2 is a two-interval computation on the cylinder. For a general two-dimensional CFT, the entropy of two intervals is not known explicitly. However, if we take the OPE limit $\sigma_1 \to 0$, we obtain (up to a divergent constant) that the entropy is just the sum of the two intervals. Hence,

$$S_m \sim \frac{c}{6}\left(\log\frac{\sin^2(2\sigma_2/2)}{\sin^2\sigma_2} + \log\frac{\sin^2(2\sigma_1/2)}{\sin^2\sigma_1}\right) = 0. \quad \text{(E2)}$$

Therefore, in this limit, we get an answer that is independent of σ_2.

The leading correction is nonuniversal; it depends on the CFT. If we consider c free Dirac fermions [60], the entanglement entropy of the two-interval region $[x_1, x_2] \cup [x_3, x_4]$ with metric $ds^2 = \Omega^{-2}dx d\bar{x}$, is

$$S_{\text{fermions}} = \frac{c}{6}\log\left[\frac{|x_{21}x_{32}x_{43}x_{41}|^2}{|x_{31}x_{42}|^2\,\Omega_1\Omega_2\Omega_3\Omega_4}\right]$$

$$\sim \frac{c}{6}\log\left[\frac{\sin^2\left(\frac{1}{2}(\theta_1-\theta_2)\right)\sin^2\left(\frac{1}{2}(\theta_2-\theta_3)\right)\sin^2\left(\frac{1}{2}(\theta_1-\theta_4)\right)\sin^2\left(\frac{1}{2}(\theta_3-\theta_4)\right)}{\sin^2\left(\frac{1}{2}(\theta_2-\theta_4)\right)\sin^2\left(\frac{1}{2}(\theta_1-\theta_3)\right)\Omega_1\Omega_2\Omega_3\Omega_4}\right]$$

$$\sim \frac{c}{6}\log\left[\frac{\sin^2\frac{1}{2}(\sigma_1-\sigma_2)}{\sin^2\frac{1}{2}(\sigma_1+\sigma_2)}\right]. \quad \text{(E3)}$$

Now, expanding around $\sigma_1 = 0$, we obtain

$$S_{\text{fermions}} \sim -\frac{c\sigma_1}{3\tan(\sigma_2/2)}. \tag{E4}$$

If we further expand σ_2 around the bifurcate horizon $\sigma_2 = \pi/2$, we obtain $S_{\text{fermions}} \sim c\sigma_1(\sigma_2 - \pi/2)/3$. As expected, the entropy will decrease if we move σ_2 closer to σ_1. A wide variety of bulk setups can be analyzed using these approximations, which we intend to report elsewhere.

---

[1] G. 't Hooft, Dimensional reduction in quantum gravity, *Conference on Highlights of Particle and Condensed Matter Physics (SALAMFEST) Trieste, Italy, March 8–12, 1993*, Conf. Proc. **C930308**, 284–296 (1993), arXiv:gr-qc/9310026 [gr-qc].

[2] L. Susskind, The world as a hologram, J. Math. Phys. **36**, 6377 (1995).

[3] J. M. Maldacena, The large N limit of superconformal field theories and supergravity, Int. J. Theor. Phys. **38**, 1113 (1999), [Adv. Theor. Math. Phys. 2, 231 (1998)].

[4] A. R. Brown, H. Gharibyan, S. Leichenauer, H. W. Lin, S. Nezami, G. Salton, L. Susskind, B. Swingle, and M. Walter, Quantum Gravity in the Lab. I. Teleportation by Size and Traversable Wormholes, PRX Quantum **4**, 010320 (2023).

[5] P. Gao, D. L. Jafferis, and A. C. Wall, Traversable wormholes via a double trace deformation, J. High Energy Phys. **2017**, 151 (2017).

[6] J. Maldacena, D. Stanford, and Z. Yang, Diving into traversable wormholes, Fortschr. Phys. **65**, 1700034 (2017).

[7] T. Goldman, R. J. Hughes, and M. M. Nieto, Experimental evidence for quantum gravity? Phys. Lett. B **171**, 217 (1986).

[8] D. N. Page and C. D. Geilker, Indirect Evidence for Quantum Gravity, Phys. Rev. Lett. **47**, 979 (1981).

[9] H. W. Lin, J. Maldacena, and Y. Zhao, Symmetries near the horizon, arXiv preprint arXiv:1904.12820 (2019).

[10] A. Almheiri, T. Hartman, J. Maldacena, E. Shaghoulian, and A. Tajdini, The entropy of Hawking radiation, arXiv:2006.06872 [hep-th] (2020).

[11] X.-L. Qi and A. Streicher, Quantum epidemiology: Operator growth, thermal effects, and SYK, J. High Energy Phys. **2019**, 12 (2019).

[12] B. Freivogel, D. A. Galante, D. Nikolakopoulou, and A. Rotundo, Traversable wormholes in AdS and bounds on information transfer, arXiv:1907.13140 [hep-th] (2019).

[13] D. Bak, C. Kim, and S.-H. Yi, Experimental probes of traversable wormholes, arXiv preprint arXiv:1907.13465 (2019).

[14] N. Bao, A. Chatwin-Davies, J. Pollack, and G. N. Remmen, Traversable wormholes as quantum channels: Exploring CFT entanglement structure and channel capacity in holography, J. High Energy Phys. **2018**, 71 (2018).

[15] N. Bao, V. P. Su, and M. Usatyuk, Wormhole traversability via quantum random walks, arXiv:1906.01672 [hep-th] (2019).

[16] K. A. Landsman, C. Figgatt, T. Schuster, N. M. Linke, B. Yoshida, N. Y. Yao, and C. Monroe, Verified quantum information scrambling, Nature **567**, 61 (2019).

[17] B. Yoshida and A. Kitaev, Efficient decoding for the Hayden-Preskill protocol, arXiv:1710.03363 (2017).

[18] B. Yoshida and N. Y. Yao, Disentangling Scrambling and Decoherence via Quantum Teleportation, Phys. Rev. X **9**, 011006 (2019).

[19] M. S. Blok, V. V. Ramasesh, T. Schuster, K. O'Brien, J. M. Kreikebaum, D. Dahlen, A. Morvan, B. Yoshida, N. Y. Yao, and I. Siddiqi, Quantum information scrambling in a superconducting qutrit processor, arXiv:2003.03307 [quant-ph] (2020).

[20] J. Maldacena, Eternal black holes in anti–de Sitter, J. High Energy Phys. **2003**, 021 (2003).

[21] G. Penington, S. H. Shenker, D. Stanford, and Z. Yang, Replica wormholes and the black hole interior, arXiv:1911.11977 [hep-th] (2019).

[22] From now on, we suppress the subscripts L and R when there is no confusion.

[23] Y Liu, Statistical behavior of the eigenvalues of random matrices (2000).

[24] sign(g) dependence is crucial from the gravitational point of view, as the wrong sign of g will not make the wormhole traversable (it will send a positive-energy shock wave and make the wormhole longer).

[25] Of course, we are not discussing precise definitions of channel capacity of channels here, which could be of independent interest.

[26] N. Lashkari, D. Stanford, M. Hastings, T. Osborne, and P. Hayden, Towards the fast scrambling conjecture, J. High Energy Phys. **2013**, 22 (2013).

[27] One can consider encoding the qubit into a code space to increase the fidelity; however, for the systems of a few hundred qubits and using simple codes, our efforts have not been successful.

[28] Leonard Susskind, Complexity and Newton's laws, arXiv preprint arXiv:1904.12819 (2019).

[29] Or, more precisely, the derivative of the size is dual to the momentum [9], but when the momentum is growing exponentially the distinction is unimportant.

[30] D. A. Roberts, D. Stanford, and A. Streicher, Operator growth in the SYK model, JHEP **06**, 122 (2018).

[31] A. R. Brown, H. Gharibyan, A. Streicher, L. Susskind, L. Thorlacius, and Y. Zhao, Falling toward charged black holes, Phys. Rev. **D98**, 126016 (2018).

[32] J. Maldacena and X.-L. Qi, Eternal traversable wormhole, arXiv preprint arXiv:1804.00491 (2018).

[33] It exactly matches the size operator when the number of carrier fermions, k, is equal to n.

[34] These operators generate Poincare time. If we choose $V \sim O_L O_R$ to be slightly more complicated so that O_L and O_R are bosonic operators, then we would obtain the alternative Hamiltonian discussed in Sec. 7 of Ref. [37].

[35] We are considering a setup where the signal is sent from early (negative) times from the left side. If we were to send the signal from the right hand side, as in Ref. [6], we would have a similar equation with P_+ and P_- interchanged.

[36] If we were to use the exact expressions from Ref. [9] for E and B instead of the approximate ones, this formula

would be exact, but the connection with simple boundary quantities is obscure.

[37] I. Kourkoulou and J. Maldacena, Pure states in the SYK model and nearly-*ads*_2 gravity, arXiv preprint arXiv:1707.02325 (2017).

[38] B. Czech, J. L. Karczmarek, F. Nogueira, and M. Van Raamsdonk, The gravity dual of a density matrix, Class. Quantum Grav. **29**, 155009 (2012).

[39] A. Almheiri, X. Dong, and D. Harlow, Bulk locality and quantum error correction in AdS/CFT, J. High Energy Phys. **2015**, 163 (2015).

[40] X. Dong, D. Harlow, and A. C. Wall, Reconstruction of Bulk Operators within the Entanglement Wedge in Gauge-Gravity Duality, Phys. Rev. Lett. **117**, 021601 (2016).

[41] D. L. Jafferis, A. Lewkowycz, J. Maldacena, and S. J. Suh, Relative entropy equals bulk relative entropy, J. High Energy Phys. **6**, 1 (2016).

[42] J. Cotler, P. Hayden, G. Penington, G. Salton, B. Swingle, and M. Walter, Entanglement Wedge Reconstruction via Universal Recovery Channels, Phys. Rev. X **9**, 031011 (2019).

[43] C.-F. Chen, G. Penington, and G. Salton, Entanglement wedge reconstruction using the Petz map, J. High Energy Phys. **2020**, 1 (2020).

[44] A. Almheiri, T. Hartman, J. Maldacena, E. Shaghoulian, and A. Tajdini, Replica wormholes and the entropy of Hawking radiation, J. High Energy Phys. **05**, 013 (2020).

[45] A. Hamilton, D. N. Kabat, G. Lifschytz, and D. A. Lowe, Local bulk operators in AdS/CFT: A Boundary view of horizons and locality, Phys. Rev. D **73**, 086003 (2006).

[46] Quantum extremal surfaces and subsets of fermions in the SYK model (2021).

[47] M. Gärttner, J. G. Bohnet, A. Safavi-Naini, M. L. Wall, J. J. Bollinger, and A. M. Rey, Measuring out-of-time-order correlations and multiple quantum spectra in a trapped-ion quantum magnet, Nat. Phys. **13**, 781 (2017).

[48] J. Li, R. Fan, H. Wang, B. Ye, B. Zeng, H. Zhai, X. Peng, and J. Du, Measuring Out-Of-Time-Order Correlators on a Nuclear Magnetic Resonance Quantum Simulator, Phys. Rev. X **7**, 031011 (2017).

[49] K. A. Landsman, C. Figgatt, T. Schuster, N. M. Linke, B. Yoshida, N. Y. Yao, and C. Monroe, Verified quantum information scrambling, Nature **567**, 61 (2019).

[50] M. K. Joshi, A. Elben, B. Vermersch, T. Brydges, C. Maier, P. Zoller, R. Blatt, and C. F. Roos, Quantum Information Scrambling in a Trapped-Ion Quantum Simulator with Tunable Range Interactions, Phys. Rev. Lett. **124**, 240505 (2020).

[51] T. Schuster, B. Kobrin, P. Gao, I. Cong, E. T. Khabiboulline, N. M. Linke, M. D. Lukin, C. Monroe, B. Yoshida, N. Y. Yao, Many-body quantum teleportation via operator spreading in the traversable wormhole protocol, arXiv:2102.00010 [quant-ph] (2022).

[52] B. Collins, Moments and cumulants of polynomial random variables on unitarygroups, the Itzykson-Zuber integral, and free probability, Int. Math. Res. Not. **2003**, 953 (2003).

[53] B. Collins and P. Śniady, Integration with respect to the Haar measure on unitary, orthogonal and symplectic group, Commun. Math. Phys. **264**, 773 (2006).

[54] We ignore the insignificant $1/n$ corrections caused by action of the coupling on the message qubits.

[55] J. S. Cotler, G. Gur-Ari, M. Hanada, J. Polchinski, P. Saad, S. H. Shenker, D. Stanford, A. Streicher, and M. Tezuka, Black holes and random matrices, J. High Energy Phys. **2017**, 118 (2017).

[56] P. Saad, S. H. Shenker, and D. Stanford, A semiclassical ramp in SYK and in gravity, arXiv preprint arXiv:1806.06840 (2018).

[57] J. Maldacena and D. Stanford, Remarks on the Sachdev-Ye-Kitaev model, Phys. Rev. D **94**, 106002 (2016).

[58] We thank Douglas Stanford for discussions and useful suggestions.

[59] P. Gao and D. L. Jafferis, A traversable wormhole teleportation protocol in the SYK model, arXiv:1911.07416 (2019).

[60] H. Casini, C. D. Fosco, and M. Huerta, Entanglement and alpha entropies for a massive Dirac field in two dimensions, J. Stat. Mech. **0507**, P07007 (2005).